Physics – Uspekhi **37** (3) 229 – 246 (1994)

REVIEWS OF TOPICAL PROBLEMS PACS numbers: 72.15.Eb; 74.70.Ad; 61.72.Bb; 72.10.Fk

Transport phenomena in metals with quantum defects

A I Morozov, A S Sigov

Contents

Abstract. The interaction of quantum defects (defectons) with the conduction electrons is considered. A systematic allowance is made for infrared renormalisations which are due to this interaction and which influence significantly the width of the energy band of defectons and their contribution to the physical properties of a metal. An analysis is made of the interaction of defectons with one another and with other defects of the crystal lattice of a metal. The processes of quantum defect clusterisation due to this interaction are studied. The temperature dependences of the transport coefficients are derived both for a metal containing both free defectons and two-level systems, which appear in a number of cases when a quantum defect is captured by a heavy immobile impurity.

1. Introduction

It is well known that many low-temperature physical (for example, transport) properties of a metal are governed by the nature and concentration of impurities. Interstitial impurities may undergo transitions from interstices they occupy initially to adjacent ones and, in general, this can occur by above-barrier and tunnel processes. Since the tunnelling probability decreases exponentially on increase in the impurity mass, it is negligible for heavy impurities, so that a transition of this kind requires an activation energy of the order of 0.1 – 10 eV. At low temperatures the probability of such a jump is negligible during a typical measurement time. This is the reason why such point defects are regarded as frozen-in at certain positions when theoretical calculations are made of the properties of a metal. The defects essentially create a static field acting on electrons. The relevant 'cross' technique of calculation of the impurity scattering time is well-known (see, for example, Ref. [1]). A system of defects of this kind is very far from equilibrium.

However, some light interstitial impurities (hydrogen isotopes, helium) remain mobile even at low temperatures and they tunnel from one equivalent interstice to another. Such quantum defects will be called defectons. In contrast to frozen-in defects, they should be regarded as the internal degrees of freedom of a crystal and they can reach an equilibrium during the duration of an experiment.

This difference in the behaviour of defects makes the interaction of electrons with defectons very different from the interaction with frozen-in heavy defects. In the former case the interaction leads to infrared divergences in the calculation of renormalised parameters of the defecton subsystem, as first pointed out by Kondo [2]. The first orders of perturbation theory are insufficient in the calculation of such renormalisations. A consistent allowance for the renormalisations within the framework of the parquet approximation leads to a nontrivial temperature dependence of the electron-subsystem relaxation time, because of the electron – defecton interaction: $\tau_{e,d} \propto T^{-g}$, where T is the temperature, $g \sim 2N^2(0)V_0^2N(0)$ is the density of the electron states on the Fermi surface, and V_0 is the 'bare' amplitude of the scattering of an electron by a defecton. A typical value of g is $\sim 0.1 - 1$ and it varies from metal to metal.

This temperature dependence of $\tau_{e,d}$, related to the evolution of the electron cloud around a defecton, is the origin of the nontrivial temperature dependences of the transport coefficients of a metal containing quantum defects in that

A I Morozov, A S Sigov Moscow Institute of Radio Engineering, Electronics, and Automation, prosp. Vernadskogo 78, 117454 Moscow
Tel. (095) 434-76-65; (095) 434-93-47
Fax (095) 434-86-65

Received 10 November 1993
Uspekhi Fizicheskikh Nauk **164** (3) 243 – 261 (1994)
Translated by A Tybulewicz

temperature range in which the scattering by defectons is the main mechanism of relaxation of the electron subsystem.

The most promising objects for the detection of such dependences are dilute transition-metal hydrides. Experimental observations of these dependences are hindered by the clusterisation of defectons which occurs at low temperatures and which is due to their interaction with one another or with heavy immobile impurities. However, in some cases the capture of a defecton by such a heavy impurity gives rise to a two-level system and a defecton partly retains its mobility even below the clusterisation temperature. Nontrivial temperature dependences can be observed in this case as well.

This review is divided into three parts. The first part (Section 2) deals with infrared renormalisations of the parameters of the defecton subsystem and of the potential of the electron – defecton interaction.

The second part (Section 3) discusses the clusterisation of mobile defects.

The third part (Section 4) is devoted to studies of anomalies of the transport coefficients of metals with quantum defects.

The summary completes the review with our conclusions and proposals.

2. Infrared renormalisations

2.1 Infrared renormalisations in an ideal crystal

The fundamental problems of quantum diffusion were discussed in the pioneering paper of A F Andreev and I M Lifshitz [3] published in 1969. In particular, they drew attention to the circumstance that at low temperatures a quantum defect in an ideal crystal is completely delocalised and can be described by a Bloch wave function. Such a description is valid in the range of temperatures in which the mean free path l_{d} of defectons exceeds considerably the interatomic spacing d. If the opposite is true, the quasimomentum becomes a 'poor' quantum number and the coordinate representation is more acceptable.

We shall consider a quantum defect in an ideally periodic potential of the crystal lattice. An interstice then represents a potential well for a defecton. As a rule, such a well contains several local vibrational levels of quantum defects. Each such level creates a narrow defecton band because of tunnelling. The small mass of a quantum defect means that the first excited level is separated from the ground state by an energy of the order of 0.1 eV [4], so that it is permissible to ignore the influence of higher levels in studies of low-temperature scattering processes. We shall understand the 'defecton band' to be a band which is formed from the ground vibrational level.

In bcc, fcc, and hcp metals there are several tetrahedral interstices for every site atom and in bcc metals there may be also several octahedral interstices. Therefore, a local energy level creates several defecton bands [5]. However, allowance for several defecton dispersion laws, separated from one another by an energy of the order of (or less than) the defecton band width, complicates greatly the calculations without altering the physical nature of the phenomena. We shall therefore consider just one nondegenerate defecton band.

The Hamiltonian of free defectons is

$$\mathcal{H}_{\mathrm{d}} = \sum_{\boldsymbol{k}} \omega(\boldsymbol{k})\, c^{+}(\boldsymbol{k})\, c(\boldsymbol{k})\,, \tag{2.1}$$

where $\omega(\boldsymbol{k})$ is the dispersion law and $c^{+}(\boldsymbol{k})$ and $c(\boldsymbol{k})$ are the defecton creation and annihilation operators. Summation over $\boldsymbol{k}$ is carried out in the first Brillouin zone.

Defectons interact with phonons, electrons, with one another, and with other lattice defects. We shall consider first the infrared renormalisations in an ideal crystal with an extremely low concentration of quantum defects when their interaction with one another and with other defects can be ignored.

The interaction of defectons with phonons causes defecton damping and gives rise to the polaron effect, which is the narrowing of the defecton band because of the deformation of the crystal lattice around a defect. The new width of the defecton band ε_0 is [6]

$$\varepsilon_0 = \varepsilon_{00}\, \mathrm{e}^{-S(T)}\,, \tag{2.2}$$

where ε_{00} is the width of the defecton band in the absence of strains and S is of the order of $S \sim u_0^2/w_0^2$, where u_0 is the displacement of the site atoms nearest to a defect and w_0 is the amplitude of the zero-point lattice vibrations. At temperatures T much lower than the Debye temperature θ the value of $S(T)$ becomes constant. We shall consider only that range of temperatures, because if $T \geqslant \theta$, the phonon contribution to relaxation of the electron subsystem exceeds the corresponding contribution of quantum defects. Therefore, we may assume that $\varepsilon_0 = \mathrm{const}$ at $T \ll \theta$ and $\omega(\boldsymbol{k})$ in Eqn (2.1) is the dispersion law of defectons which allows for the defecton – phonon interaction.

In normal metals at temperatures $T \ll \theta$ the main contribution to the damping of defectons comes from their scattering by the conduction electrons [7] and the phonon contribution to relaxation of the defecton subsystem considered earlier [3] may become important only in a super-conductor at temperatures $T \ll T_{\mathrm{c}}$ (T_{c} is the superconducting transition temperature), when the number of electronic excitations is exponentially small.

We shall now consider the electron – defecton interaction. We shall investigate the range of low temperatures when quantum defects in a metal are delocalised and are described by the Bloch wave functions.

The Hamiltonians of the conduction electrons $\mathcal{H}_{\mathrm{e}}$ and of the electron – defecton interaction $\mathcal{H}_{\mathrm{e-d}}$ are

$$\mathcal{H}_{\mathrm{e}} = \sum_{\boldsymbol{k}} \varepsilon(\boldsymbol{k}) a^{+}(\boldsymbol{k}) a(\boldsymbol{k})\,, \tag{2.3}$$

$$\mathcal{H}_{\mathrm{e-d}} = \sum_{\boldsymbol{k},\boldsymbol{k}',\boldsymbol{q}} V_0(\boldsymbol{q}) a^{+}(\boldsymbol{k}'-\boldsymbol{q}) c^{+}(\boldsymbol{k}+\boldsymbol{q}) c(\boldsymbol{k}) a(\boldsymbol{k}')\,, \tag{2.4}$$

where $\varepsilon(\boldsymbol{k})$ is the dispersion law, $a^{+}(\boldsymbol{k})$ and $a(\boldsymbol{k})$ are the second-quantisation operators of the conduction electrons, and $V_0(\boldsymbol{q})$ is the bare amplitude of the scattering of an electron by a defecton.

The total Hamiltonian of the system under discussion is the sum of $\mathcal{H}_{\mathrm{d}}$, $\mathcal{H}_{\mathrm{e}}$, and $\mathcal{H}_{\mathrm{e-d}}$.

We shall consider the electron – defecton interaction on the basis of the temperature diagram technique [1]. We shall assume that defectons obey the Fermi statistics. This assumption is not essential, because we shall as a rule consider a nondegenerate gas of defectons and the Boltzmann limit is the same for the Fermi and Boltzmann statistics.

The zeroth-order Green functions of electrons and defectons, which will be represented by thin continuous and dashed lines, are respectively:

$$G_0(\boldsymbol{k},\ \varepsilon_k) = \left[\mathrm{i}\varepsilon_k - \varepsilon(\boldsymbol{k}) + \mu\right]^{-1}, \tag{2.5}$$

$$\Psi_0(\boldsymbol{k},\ \varepsilon_k) = \left[\mathrm{i}\varepsilon_k - \omega(\boldsymbol{k}) + \zeta\right]^{-1}, \tag{2.6}$$

where $\varepsilon_k = \pi T(2k+1)$ is the Matsubara frequency, and μ and ζ are the chemical potentials of electrons and defectons. The interaction $V_0(\boldsymbol{q})$ is represented by a wavy line.

We shall first discuss the defecton self-energy part $\chi(\boldsymbol{k}, \varepsilon_k)$ on the assumption that the reaction of the defecton on the electron subsystem can be ignored because of the low concentration of defectons.

The graph shown in Fig. 1a shows only the renormalisation of ζ, whereas the graph in Fig. 1b gives not only the renormalisation of ζ, but also the contribution made to the defecton damping [7]. The contribution of this diagram to $\chi(\boldsymbol{k},\ \varepsilon_k)$ is

$$\chi_1(\boldsymbol{k}\varepsilon_k) = -2T^2 \sum_{\varepsilon_m, \omega_n} \int \frac{\mathrm{d}\boldsymbol{q}\,\mathrm{d}\boldsymbol{k}'}{(2\pi)^6} |V_0(\boldsymbol{q})|^2 G_0(\boldsymbol{k}'-\boldsymbol{q},\ \varepsilon_m - \omega_n) \times G_0(\boldsymbol{k}',\ \varepsilon_m) \Psi_0(\boldsymbol{k}-\boldsymbol{q},\ \varepsilon_k - \omega_n)\,. \tag{2.7}$$

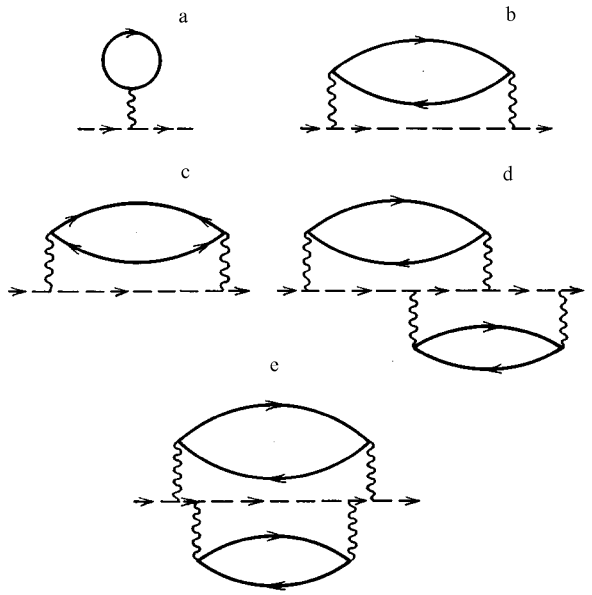

Figure 1. Diagrams of the self-energy part of the defecton Green function $\chi(\boldsymbol{k}, \varepsilon_k)$.

After summation over the frequencies we find that

$$\chi_1(\boldsymbol{k},\ \varepsilon_k) = 2\int \frac{\mathrm{d}\boldsymbol{q}\,\mathrm{d}\boldsymbol{k}'}{(2\pi)^6} |V_0(\boldsymbol{q})|^2 \times \frac{n(\boldsymbol{k}'-\boldsymbol{q})\,[1-n(\boldsymbol{k}')]}{\mathrm{i}\varepsilon_k - \varepsilon(\boldsymbol{k}') + \varepsilon(\boldsymbol{k}'-\boldsymbol{q}) - \omega(\boldsymbol{k}-\boldsymbol{q}) + \zeta}\,, \tag{2.8}$$

where

$$n(\boldsymbol{k}) = \{1 + \exp[(\varepsilon(\boldsymbol{k}) - \mu)T^{-1}]\}^{-1} \tag{2.9}$$

is the Fermi electron distribution function.

The imaginary part of χ_1 can be found by analytic continuation of $\chi_1(\boldsymbol{k}, \varepsilon_k)$ from points $\varepsilon = \mathrm{i}\varepsilon_k$ to the real part and integration near a pole. If $T \gg \varepsilon_0$, the value of $\omega(\boldsymbol{k})$ can be ignored in comparison with the characteristic values $|\varepsilon(\boldsymbol{k}') - \varepsilon(\boldsymbol{k}'-\boldsymbol{q})| \sim T$, so that

$$\mathrm{Im}\,\chi_1 = -\pi g T\,, \tag{2.10}$$

where

$$g = 2\int \frac{\mathrm{d}\boldsymbol{k}\ \mathrm{d}\boldsymbol{k}' |V_0(\boldsymbol{k}-\boldsymbol{k}')|^2}{(2\pi)^6 |\nabla\varepsilon(\boldsymbol{k})| \cdot |\nabla\varepsilon(\boldsymbol{k}')|} \tag{2.11}$$

and integration with respect to $\boldsymbol{k}$ and $\boldsymbol{k}'$ is carried out over the Fermi surface.

If $T \ll \varepsilon_0$, the imaginary part is of the order of $\mathrm{Im}\,\chi_1 = -\pi g T^2/\varepsilon_0$, since the electron quasimomentum can change only by the value $\tilde{k} \sim k_{\mathrm{B}}(T/\varepsilon_0)^{1/2}$, which is the quasimomentum of a defecton with a thermal energy T (k_{B} is the Brillouin quasimomentum). This leads to a reduction in the phase volume of the final states of an electron and to a faster fall of $\mathrm{Im}\,\chi_1$ with temperature.

In a superconductor the number of electronic excitations decreases rapidly as a result of cooling. At temperatures $T \ll T_{\mathrm{c}}$, where T_{c} is the superconducting transition temperature, this number is exponentially small. We can calculate $\chi_1(\boldsymbol{k}, \varepsilon_k)$ for a superconductor if, in addition to the loops formed by the normal Green functions of electrons $G_0(\boldsymbol{k}, \varepsilon_m)$ (Fig. 1b), allowance is made for the loops with the anomalous Green functions of electrons $F(\boldsymbol{k}, \varepsilon_m)$ and $F^+(\boldsymbol{k}, \varepsilon_m)$. In the absence of an electromagnetic field the Green functions of electrons in a superconductor are

$$F(\boldsymbol{k},\ \varepsilon_k) = F^+(\boldsymbol{k},\ \varepsilon_k) = \frac{\Delta}{\varepsilon_k^2 + (\varepsilon(\boldsymbol{k}) - \mu)^2 + \Delta^2}\,, \tag{2.12}$$

$$G_0(\boldsymbol{k},\ \varepsilon_k) = -\frac{\mathrm{i}\varepsilon_k + \varepsilon(\boldsymbol{k}) - \mu}{\varepsilon_k^2 + (\varepsilon(\boldsymbol{k}) - \mu)^2 + \Delta^2}\,, \tag{2.13}$$

where Δ is the gap in the spectrum of electronic excitations [1]. The anomalous Green functions make a contribution to $\chi_1(\boldsymbol{k}, \varepsilon_k)$ shown in Fig. 1c and the continuous curves with two incoming and outgoing arrows correspond to the anomalous Green functions $F(\boldsymbol{k}, \varepsilon_m)$ and $F^+(\boldsymbol{k}, \varepsilon_m)$.

The value of $\chi_1(\boldsymbol{k}, \varepsilon_k)$ for a superconductor is [8, 9]

$$\begin{aligned}\chi_1^{\mathrm{s}}(\boldsymbol{k},\ \varepsilon_k) = 2\int \frac{\mathrm{d}\boldsymbol{k}_1 \mathrm{d}\boldsymbol{k}_2 |V_0(\boldsymbol{k}_1 - \boldsymbol{k}_2)|^2}{(2\pi)^6 |\nabla\varepsilon(\boldsymbol{k}_1)| \cdot |\nabla\varepsilon(\boldsymbol{k}_2)|} \int_{\Delta}^{E_0} \mathrm{d}\varepsilon_1 \\ \times \int_{\Delta}^{E_0} \mathrm{d}\varepsilon_2 v(\varepsilon_1) v(\varepsilon_2) \Bigg\{ \frac{n(\varepsilon_1)\,[1-n(\varepsilon_2)]\,(\varepsilon_1\varepsilon_2 - \Delta^2)}{\mathrm{i}\varepsilon_{\mathrm{k}} - \omega(\boldsymbol{k}+\boldsymbol{k}_1-\boldsymbol{k}_2) + \varepsilon_1 - \varepsilon_2} \\ + \frac{n(\varepsilon_2)\,[1-n(\varepsilon_1)]\,(\varepsilon_1\varepsilon_2 - \Delta^2)}{\mathrm{i}\varepsilon_{\boldsymbol{k}} - \omega(\boldsymbol{k}+\boldsymbol{k}_1-\boldsymbol{k}_2) - \varepsilon_1 + \varepsilon_2} \\ + \frac{n(\varepsilon_1)\,n(\varepsilon_2)\,(\varepsilon_1\varepsilon_2 + \Delta^2)}{\mathrm{i}\varepsilon_k - \omega(\boldsymbol{k}+\boldsymbol{k}_1-\boldsymbol{k}_2) + \varepsilon_1 + \varepsilon_2} \\ + \frac{[1-n(\varepsilon_1)]\,[1-n(\varepsilon_2)]\,(\varepsilon_1\varepsilon_2 + \Delta^2)}{\mathrm{i}\varepsilon_k - \omega(\boldsymbol{k}+\boldsymbol{k}_1-\boldsymbol{k}_2) - \varepsilon_1 - \varepsilon_2} \Bigg\}\,,\end{aligned} \tag{2.14}$$

where $v(\varepsilon) = (\varepsilon^2 - \Delta^2)^{-1/2}$ and E_0 is the half-width of the electron band.

If the imaginary part $\chi_1^{\mathrm{s}}(\boldsymbol{k}, \varepsilon)$ is obtained from Eqn (2.14), the result is

$$\mathrm{Im}\,\chi_1^{\mathrm{s}}(T) = -2\pi g T\,\{1 + \exp[\Delta(T)T^{-1}]\}^{-1}\,. \tag{2.15}$$

We are continuing to assume that $\max(T, \Delta) \gg \varepsilon_0$. We shall now consider the real part of $\chi(\boldsymbol{k}, \varepsilon)$. Integration in Eqns (2.8) and (2.14) over the range of values of $\boldsymbol{k}_1$ and $\boldsymbol{k}_2$ far from the Fermi surface, in combination with the renormalisation of η, gives — as demonstrated by Kondo [2] — also the real part $\chi_1(\boldsymbol{k}, \varepsilon)$ dependent on $\boldsymbol{k}$ and ε and the nature of this function is largely determined by the dispersion law of defectons. Here $\chi_1(\boldsymbol{k}, \varepsilon)$ is the result of analytic continuation of the function $\chi_1(\boldsymbol{k}, \varepsilon_k)$ from the points $\varepsilon = \mathrm{i}\varepsilon_k$ to the real axis.

If $T \gg \varepsilon_0$, the answer is readily obtained by expanding the denominator of Eqn (2.8) in powers of ε and of $[\omega(\boldsymbol{k}) - \zeta]$. With logarithmic accuracy, i.e. if we allow only for the terms leading in $\ln(E_0/T)$, the result is

$$\mathrm{Re}\,\chi_1(\boldsymbol{k},\ \varepsilon) = \delta\zeta - [g(\varepsilon+\zeta) - I_1]\ln(E_0 T^{-1}), \qquad (2.16)$$

where $\delta\zeta$ is the result of renormalisation of the chemical potential and

$$I_1 = 2\int \frac{\mathrm{d}\boldsymbol{k}_1\,\mathrm{d}\boldsymbol{k}_2 |V_0(\boldsymbol{k}_1 - \boldsymbol{k}_2)|^2}{(2\pi)^6 |\nabla\varepsilon(\boldsymbol{k}_1)|\cdot|\nabla\varepsilon(\boldsymbol{k}_2)|}\,\omega(\boldsymbol{k} - \boldsymbol{k}_1 + \boldsymbol{k}_2), \qquad (2.17)$$

where integration over $\boldsymbol{k}_1$ and $\boldsymbol{k}_2$ is carried out over the Fermi surface.

If the dispersion law $\omega(\boldsymbol{k})$ is quadratic, the integral is $I_1 = g\omega(\boldsymbol{k})$, and in the tight-binding case [2] it becomes $I_1 = m\omega(\boldsymbol{k})$, where m is given by [2, 10]

$$m = 2\int \frac{\mathrm{d}\boldsymbol{k}\,\mathrm{d}\boldsymbol{k}' |V_0(\boldsymbol{k} - \boldsymbol{k}')|^2 \cos[(\boldsymbol{k} - \boldsymbol{k}')\cdot\boldsymbol{a}]}{(2\pi)^6 |\nabla\varepsilon(\boldsymbol{k})|\cdot|\nabla\varepsilon(\boldsymbol{k}')|} \qquad (2.18)$$

and $\boldsymbol{a}$ is the position vector connecting two nearest interstices of a given type. A more rigorous calculation in the case of an arbitrary relationship between ε_0 and T gives, instead of $\ln(E_0/T)$ in Eqn (2.16), $\ln[E_0/\max(T,\varepsilon_0)]$ for a normal metal and $\ln[E_0/\max(T,\varepsilon_0,\Delta)]$ for a superconductor. The logarithmic divergence for a superconductor is related to the last term in the braces in Eqn (2.14). Similar logarithmic terms appear also when corrections to $V_0(\boldsymbol{q})$ are calculated.

In general, the logarithm does not contain ε_0 but $\varepsilon_0(k_\mathrm{F}/k_\mathrm{B})^2$, where k_F is the Fermi momentum, but for metals we have $k_\mathrm{F} \sim k_\mathrm{B}$, so that we can drop the factor $(k_\mathrm{F}/k_\mathrm{B})^2$.

If the scattering of an electron by a defecton is accompanied by the transition of the latter to the next vibrational level, the logarithmic divergence in Eqn (2.16) is cut off not at $\max(T,\varepsilon_0)$, but at the difference $\hbar\omega_0$ between the vibrational energies. Since temperatures $T \ll \theta$ we have $\ln(E_0/\hbar\omega_0) \ll \ln[E_0/\max(T,\varepsilon_0)]$, we shall ignore the contribution made to $\mathrm{Re}\,\chi(\boldsymbol{k},\varepsilon)$ by transitions between the vibrational energy levels of a defecton.

The infrared divergence of $\chi(\boldsymbol{k},\ \varepsilon)$ is related to the presence of a steep edge of the Fermi electron distribution, i.e. it is related to the existence of electron–hole pairs with a low energy, and is cut off at a value corresponding to spreading of this edge T or at ε_0. The energy of electron–hole pairs and, consequently,the logarithmic divergence are limited from below by the value of 2Δ in the case of superconductors.

The strong renormalisation of the defecton Green function is a consequence of the electron polaron effect: the existence of an electron cloud around a defecton alters considerably its characteristics.

It seems desirable to sum up all the most divergent terms of the perturbation theory series and go beyond the constraints set by $g\ln[E_0/\max(T,\varepsilon_0)] \ll 1$. An attempt to carry out such summation was undertaken in Refs [11, 2]. However, the treatment given there suffers from a number of serious shortcomings. It is well known that the parquet diagrams contain the largest degree of a diverging logarithm. The first parquet diagrams which dominate the contribution to $\chi(\boldsymbol{k},\varepsilon)$ and the renormalisation of $V_0(\boldsymbol{q})$ in a normal metal are shown in Figs 1b, 1d, 1e, and Fig. 2, respectively.

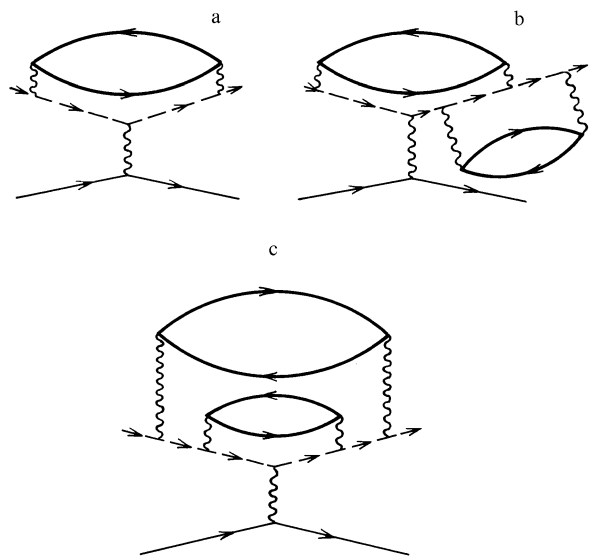

Figure 2. Diagrams of the vertex of the electron–defecton interaction $V(\boldsymbol{q})$.

In calculation of the total amplitude of the scattering of an electron by a defecton $V(\boldsymbol{q})$ in Ref. [11], which has been used in later papers, it is assumed that the main contribution to the renormalisation of $V_0(\boldsymbol{q})$ is made by the diagrams in which all the electron loops enclose a 'bare' vertex. Allowance is made for nonparquet diagrams of the type shown in Fig. 3, but not for parquet diagrams of the type shown in Fig. 2b [9].

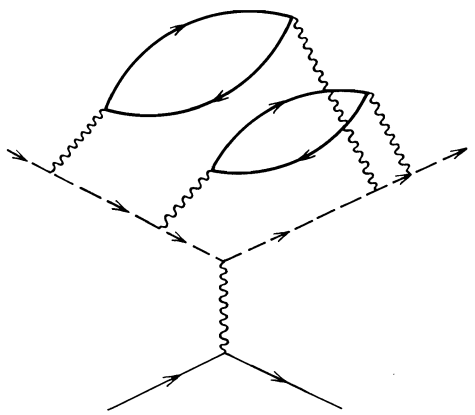

Figure 3. Nonparquet diagram for the vertex of the electron–defecton interaction $V(\boldsymbol{q})$.

A consistent allowance for the parquet diagrams has been made [12–14] in a similar, in respect of the technique, problem of calculation of the anomalies of the absorption of X-rays in metals and their emission from metals. As demonstrated in these papers, logarithmically diverging corrections of the order of $g^{1/2}\ln[E_0/\max(T,\varepsilon_0)]$ to $V_0(\boldsymbol{q})$, which originate from the diagrams shown in Fig. 4, compensate one another. Such compensation occurs in all the orders of perturbation theory. Therefore, the first nonvanishing terms containing a large logarithm are of the order of $g\ln[E_0/\max(T,\varepsilon_0)]$.

Summation of the parquet diagrams, carried out in a manner similar to that adopted in Refs [12–14], yields the following expressions for the renormalised Green function of

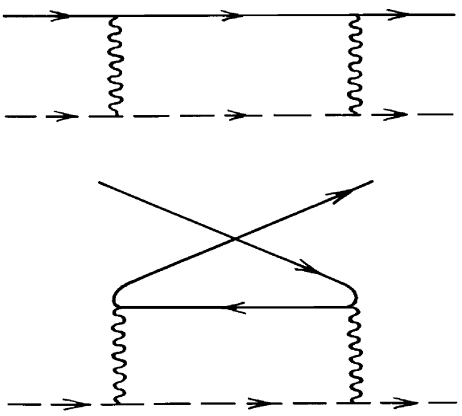

Figure 4. Diagrams leading to logarithmically diverging corrections of the order of $g^{1/2}\ln[E_0/\max(\varepsilon_0, T)]$ to the vertex $V_0(\boldsymbol{q})$.

defectons $\psi(\boldsymbol{k}, \varepsilon_k)$ and for the total vertex of the electron–defecton interaction $V(\boldsymbol{q})$:

$$\Psi(\boldsymbol{k},\ \varepsilon_k) = [\mathrm{i}\varepsilon_k - \tilde{\omega}(\boldsymbol{k}) + \zeta]^{-1}\left[\frac{\max(T,\ \varepsilon_0)}{E_0}\right]^g, \qquad (2.19)$$

where $\tilde{\omega}(\boldsymbol{k})$ is the renormalised dispersion law of defectons and

$$V(\boldsymbol{q}) = V_0(\boldsymbol{q})\left[\frac{E_0}{\max(T, \varepsilon_0)}\right]^g. \qquad (2.20)$$

The diagrams for the self-energy part of the defecton Green function $\chi(\boldsymbol{k}, \varepsilon_k)$ and $V(\boldsymbol{q})$ are plotted in Figs 5 and 6, respectively. The double dashed line corresponds to $\Psi(\boldsymbol{k}, \varepsilon_k)$, and the wavy line with a black triangle at its end is $V(\boldsymbol{q})$.

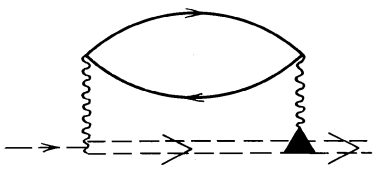

Figure 5. Diagram of the self-energy part of the defecton Green function $\chi(\boldsymbol{k}, \varepsilon_k)$.

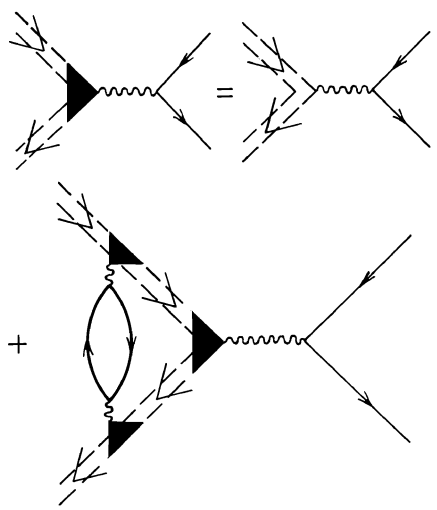

Figure 6. Diagram of the complete vertex of the electron–defecton interaction.

In these calculations we need to allow for the fact that the divergence is cut off at $\max(T, \varepsilon_0, \eta)$, where η is the highest of the frequencies that occur in the Green function vertex, measured from the level of the corresponding chemical potential. We shall be interested in the values of the Green function near the mass surfaces where $\eta \sim T$.

In spite of the fact that not all the parquet diagrams are summed in Refs [2, 11], the final result is correct.

The analysis reported in Refs [12–14] applies to a dispersion-free hole (electron) at a deep level, so that renormalisation of the dispersion law has not been considered. Since the width of the defecton band is the most important parameter in an investigation of the behaviour of a quantum particle, we shall deal in greater detail with the renormalisation of the dispersion law.

The Ward identity makes it possible to find the relationship between the quantity

$$\frac{\partial\chi(\boldsymbol{k},\ \varepsilon_m)}{\partial\boldsymbol{k}} = v\frac{\partial\chi(\boldsymbol{k},\ \varepsilon_m)}{\partial\omega(\boldsymbol{k})}$$

and a certain vertex $\Lambda(\boldsymbol{k}, \varepsilon_m)$, which differs from $V(\boldsymbol{q})$ because instead of the 'bare' vertex it contains the defecton velocity $v = \partial\omega(\boldsymbol{k})/\partial\boldsymbol{k}$ (see, for example, Ref. [15]):

$$\Lambda(\boldsymbol{k}, \varepsilon_m) = v\left(1 + \frac{\partial\chi(\boldsymbol{k}, \varepsilon_m)}{\partial\omega(\boldsymbol{k})}\right). \qquad (2.21)$$

The Bethe–Salpeter equation for $\Lambda(\boldsymbol{k}, \varepsilon_m)$ shown graphically in Fig. 7 is

$$\Lambda(\boldsymbol{k},\ \varepsilon_k) = v - 2T^2\sum_{\varepsilon_m,\,\varepsilon_n}\int\frac{\mathrm{d}\boldsymbol{p}\,\mathrm{d}\boldsymbol{p}'}{(2\pi)^6}|V_0(\boldsymbol{p}-\boldsymbol{p}')|^2$$
$$\times G_0(\boldsymbol{p}, \varepsilon_m)G_0(\boldsymbol{p}', \varepsilon_n)\Psi_0^2(\boldsymbol{k}-\boldsymbol{p}+\boldsymbol{p}', \varepsilon_k - \varepsilon_m + \varepsilon_n)$$
$$\times\Lambda(\boldsymbol{k}-\boldsymbol{p}+\boldsymbol{p}',\ \varepsilon_k - \varepsilon_m + \varepsilon_n). \qquad (2.22)$$

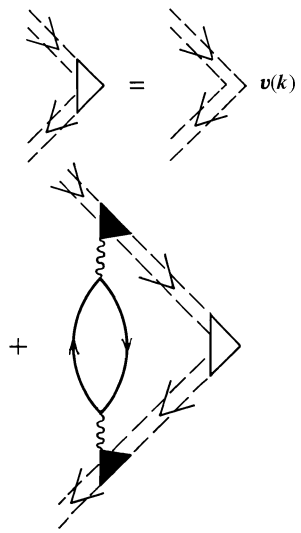

Figure 7. Diagram of a vector vertex.

Allowance is made here for the fact that the renormalisation of the defecton Green functions compensates for the renormalisation of $V_0(\boldsymbol{q})$ and, as shown below, we can ignore the change in the dispersion law of defectons in the denominator of $\psi_0(\boldsymbol{k}, \varepsilon_k)$ when the parquet approximation is used.

We shall now compare the ladder diagrams for the vertex $\boldsymbol{\Lambda}(\boldsymbol{k},\varepsilon_k)$ with the corresponding diagrams for $V(\boldsymbol{k})$, [they are obtained after compensation for the renormalisations of $\boldsymbol{\Psi}_0(\boldsymbol{k},\varepsilon_k)$ and $V_0(\boldsymbol{k})$; see Fig. 6].

If the dispersion law of defectons is quadratic, the terms in the series for $\boldsymbol{\Lambda}(\boldsymbol{k},\varepsilon_k)$ are proportional to the terms of the corresponding series for $V(\boldsymbol{k})$:

$$\frac{\boldsymbol{\Lambda}(\boldsymbol{k},\varepsilon_k)}{V(\boldsymbol{k})}=\frac{v}{V_0(\boldsymbol{k})}. \tag{2.23}$$

We finally obtain

$$1+\frac{\partial\chi(\boldsymbol{k},\varepsilon_m)}{\partial\omega(\boldsymbol{k})}=\left[\frac{E_0}{\max(T,\varepsilon_0)}\right]^g. \tag{2.24}$$

It therefore follows that if the dispersion law of defectons is quadratic, there is no renormalisation of this law and the electron – defecton interaction changes only the residue of the Green function of defectons [2].

In the tight-binding approximation, which corresponds to a real situation, each integration with respect to $\boldsymbol{p}$ and $\boldsymbol{p}'$ gives a factor m in the series for $\boldsymbol{\Lambda}(\boldsymbol{k},\varepsilon_k)$ and a factor g in the series for $V(\boldsymbol{k})$. Therefore, the quantity $\boldsymbol{\Lambda}(\boldsymbol{k},\varepsilon_k)$ can be obtained from $V(\boldsymbol{k})$ by the replacement of $V_0(\boldsymbol{k})$ with v and of g with m:

$$1+\frac{\partial\chi(\boldsymbol{k},\varepsilon_k)}{\partial\omega(\boldsymbol{k})}=\left[\frac{E_0}{\max(T,\varepsilon_0)}\right]^m. \tag{2.25}$$

The final result obtained subject to Eqn (2.19) is

$$\widetilde{\omega}(\boldsymbol{k})=\omega(\boldsymbol{k})\left[\frac{\max(T,\varepsilon_0)}{E_0}\right]^\beta, \tag{2.26}$$

where

$$\beta=g-m. \tag{2.27}$$

Kondo [2] gave the correct final expressions for $\omega(\boldsymbol{k})$, but a rigorous derivation of this result is missing.

As expected, the polaron effect reduces the width of the defecton band:

$$\widetilde{\varepsilon}_0=\varepsilon_0\left[\frac{\max(T,\varepsilon_0)}{E_0}\right]^\beta. \tag{2.28}$$

At $T=0$, on the assumption that all the electrons can match adiabatically the motion of a quantum defect, we find that $\widetilde{\varepsilon}_0$ vanishes. This is what is known as the Anderson 'orthogonalisation catastrophe' [16]. However, electrons of energy less than $\widetilde{\varepsilon}_0$ cannot follow adiabatically the motion of a defecton and, therefore, the width of the defecton band remains finite.

Experimental results discussed later can be used to demonstrate that the value of $\widetilde{\varepsilon}_0$ for hydrogen in some transition metals is of the order of 1 – 10 K. The value of $\widetilde{\varepsilon}_0$ for deuterium is approximately an order of magnitude less.

In some cases a self-consistent solution has been obtained [10, 17, 18] by replacing ε_0 in the expression (T,ε_0) with $\widetilde{\varepsilon}_0$, which corresponds to allowance for the renormalisation of the dispersion law in the Green functions of defectons when integration is carried out in Eqn (2.22) and is equivalent to the replacement of β with $\beta/(1-\beta)$ in Eqn (2.28) if $T<\widetilde{\varepsilon}_0$. However, this replacement exceeds the precision of the parquet approximation which is valid in the range where

$$g^{3/2}\ln\left\{E_0[\max(T,\varepsilon_0)]^{-1}\right\}\ll 1. \tag{2.29}$$

Yu M Kagan and N V Prokof'ev used the adiabatic approximation to obtain the following estimate of the renormalised width of the defecton band [51]:

$$\widetilde{\varepsilon}_0=\varepsilon_{\mathrm{ad}}[\max(\widetilde{\varepsilon}_0,T)(\hbar\omega_0)^{-1}]^\beta, \tag{2.30}$$

where ω_0 is the local frequency of vibrations of a defect at an interstice. The apparent discrepancy between Eqns (2.28) and (2.30) is due to the different selection of the initial approximation for the defecton band width. If ε_0 corresponds to defectons that do not interact with electrons, the adiabatic approximation allows for the interaction with electrons the energy of which exceeds $\hbar\omega_0$. Therefore, (see, for example, Ref. [19])

$$\varepsilon_{\mathrm{ad}}=\varepsilon_0(\hbar\omega_0E_0^{-1})^\beta, \tag{2.31}$$

and Eqns (2.28) and (2.30) are equivalent within the range of validity of the parquet approximation.

Yamada and his colleagues [18, 20, 21] have investigated the probability of a transition of a quantum defect, localised (in the absence of disorder) at the moment $t=0$ in a given interstice, to a state which is localised in the next interstice. By analogy with Ref. [14], the dependence of the probability of a jump on the phase shift of the scattered wave of an electron on the Fermi surface is found for the case when there is only s-scattering of electrons by defectons. This is done for an arbitrary strength of the defecton – electron interaction. In the range where the interaction is weak $[N(0)V_0\ll 1]$ the expression obtained is similar to Eqn (2.28). Taken as a whole, this dynamical problem is not equivalent to that discussed here.

The above discussion is based on the assumption of the band nature of defecton motion. The condition $l_{\mathrm{d}}\gg d$ is equivalent to $\tau_{\mathrm{d}}\widetilde{\varepsilon}_0\gg 1$ (it is assumed that $\hbar\equiv 1$), where τ_{d} is the mean free time of a defecton given by

$$\tau_{\mathrm{d}}^{-1}=-2\,\mathrm{Im}\,\chi(\boldsymbol{k},\varepsilon). \tag{2.32}$$

We can easily see that this condition is satisfied by normal metals at temperatures

$$T\ll\frac{\widetilde{\varepsilon}_0}{2\pi g} \tag{2.33}$$

which for real values of g corresponds to $T\ll\widetilde{\varepsilon}_0$.

In the superconducting phase we have $\tau_{\mathrm{d}}\widetilde{\varepsilon}_0\gg 1$ at temperatures $T\ll T_{\mathrm{c}}$. In this temperature range the phonon contribution to τ_{d}^{-1} may predominate. The order of magnitude of this contribution is

$$\tau_{\mathrm{d,ph}}^{-1}=T(T\theta^{-1})^6. \tag{2.34}$$

The temperature dependence of the corresponding time was found by Andreev and Lifshitz [3].

On increase in temperature the mean free path of a defecton becomes less than the interatomic spacing and the motion of a defecton becomes of hopping nature.

A satisfactory microscopic description of defectons with controlled parameters of the adopted approximations is not yet available for this range of temperatures.

We shall now consider the infrared renormalisations in the simpler case when the defecton states are localised because of statistical disorder associated with the nonideal nature of a crystal.

2.2 Infrared renormalisations in the case of localised defecton states

The presence of defects in a crystal gives rise to random shifts of the energy levels at interstices. We shall consider the situation when the shift ξ is much greater than ε_0; in this

case a defecton is localised to a good accuracy in a specific interstice. We shall also assume that $\xi \ll E_0$ and that electrons in a metal are delocalised and can be described by the Bloch functions [22, 23].

The Hamiltonians $\mathcal{H}_{\rm d}$ and $\mathcal{H}_{\rm e-d}$, considered in the site approximation for defectons, are

$$\mathcal{H}_{\rm d} = \sum_{\boldsymbol{n}} W(\boldsymbol{n})\, c^{+}(\boldsymbol{n})\, c(\boldsymbol{n}) + \tilde{t}_0 \sum_{\boldsymbol{n},\boldsymbol{\delta}} c^{+}(\boldsymbol{n}+\boldsymbol{\delta})\, c(\boldsymbol{n}), \quad (2.35)$$

$$\mathcal{H}_{\rm e-d} = \sum_{\boldsymbol{k},\boldsymbol{k}',\boldsymbol{n},\boldsymbol{\delta}} V^{(0)}_{\boldsymbol{n},\boldsymbol{n}+\boldsymbol{\delta}}(\boldsymbol{k}-\boldsymbol{k}')\, a^{+}(\boldsymbol{k})\, c^{+}(\boldsymbol{n}+\boldsymbol{\delta})\, c(\boldsymbol{n})\, a(\boldsymbol{k}') + \sum_{\boldsymbol{k},\boldsymbol{k}',\boldsymbol{n}} V^{(0)}_{\boldsymbol{n},\boldsymbol{n}}(\boldsymbol{k}-\boldsymbol{k}')\, a^{+}(\boldsymbol{k})\, c^{+}(\boldsymbol{n})\, c(\boldsymbol{n})\, a(\boldsymbol{k}'), \quad (2.36)$$

where

$$V^{(0)}_{\boldsymbol{n},\boldsymbol{n}'}(\boldsymbol{k}-\boldsymbol{k}') = \langle \boldsymbol{n}|V_0(\boldsymbol{k}-\boldsymbol{k}')\, \exp[\mathrm{i}\,(\boldsymbol{k}-\boldsymbol{k}')\boldsymbol{R}]|\boldsymbol{n}'\rangle, \quad (2.37)$$

$\boldsymbol{n}$ is a three-dimensional vector which is an integer and which specifies the position of an interstice; $W(\boldsymbol{n})$ is the energy of a defecton at an interstice; $c^{+}(\boldsymbol{n})$ and $c(\boldsymbol{n})$ are the second-quantisation operators of defectons in the site representation; $\tilde{t}_0$ is a matrix element of the tunnelling process; $\boldsymbol{\delta}$ has a range of values for the nearest neighbours; $|\boldsymbol{n}\rangle$ is the ψ function of a defecton at an interstice $\boldsymbol{n}$, specified in the coordinate space $\boldsymbol{R}$.

The Hamiltonian $\mathcal{H}_{\rm d}$ allows for the presence of diagonal disorder. In the absence of disorder, when $W(\boldsymbol{n}) = \text{const}$ and all the interstices are equivalent, $\mathcal{H}_{\rm d}$ becomes diagonal in the Bloch function representation. This case is discussed in the preceding section.

The typical value of ξ is

$$\xi = \langle |W(\boldsymbol{n}) - W(\boldsymbol{n}+\boldsymbol{\delta})|\rangle, \quad (2.38)$$

where the angular brackets denote averaging over $\boldsymbol{n}$ and $\boldsymbol{\delta}$. In view of the inequality $\xi \gg \tilde{t}_0$, to the overlap integral for the ψ functions of the states, centred at adjacent interstices, contains a small parameter $\tilde{t}_0/\xi$, and $V^{(0)}_{\boldsymbol{n},\boldsymbol{n}+\boldsymbol{\delta}}(\boldsymbol{k})$ is of the order of $\tilde{t}_0 V^{(0)}_{\boldsymbol{n},\boldsymbol{n}}(\boldsymbol{k})/\xi$.

Therefore, the main contribution to the infrared renormalisation of $V^{(0)}_{\boldsymbol{n},\boldsymbol{n}'}(\boldsymbol{k})$ and to the Green function of defectons

$$\Psi^{(0)}_{\boldsymbol{n},\boldsymbol{n}}(\varepsilon_k) = [\mathrm{i}\varepsilon_k - W(\boldsymbol{n}) + \zeta]^{-1} \quad (3.29)$$

is made by the term in Eqn (2.36) which is diagonal in $\boldsymbol{n}$. As in the absence of disorder, the first terms of the perturbation theory series for $\psi_{\boldsymbol{n},\boldsymbol{n}}(\varepsilon_k)$ and $V_{\boldsymbol{n},\boldsymbol{n}'}(\boldsymbol{k})$ are represented by the diagrams in Figs 1 and 2, where all the wavy lines (with the exception of the 'bare' vertex in Fig. 2) correspond to $V^{(0)}_{\boldsymbol{n},\boldsymbol{n}}(\boldsymbol{k})$.

An analysis similar to that given in the preceding section and carried out in the parquet approximation shows that, to within $(\tilde{t}_0/\xi)^2$, we have

$$V_{\boldsymbol{n},\boldsymbol{n}}(\boldsymbol{k}) = V^{(0)}_{\boldsymbol{n},\boldsymbol{n}}(\boldsymbol{k})\,(E_0\, T^{-1})^{g}, \quad (2.40)$$

$$V_{\boldsymbol{n},\boldsymbol{n}+\boldsymbol{\delta}}(\boldsymbol{k}) = V^{(0)}_{\boldsymbol{n},\boldsymbol{n}+\boldsymbol{\delta}}(\boldsymbol{k})\left[\frac{E_0}{\max(T,\xi)}\right]^{m}, \quad (2.41)$$

$$\Psi_{\boldsymbol{n},\boldsymbol{n}}(\varepsilon_k) = \Psi^{(0)}_{\boldsymbol{n},\boldsymbol{n}}(\varepsilon_k)\,(TE_0^{-1})^{g}, \quad (2.42)$$

$$\tilde{t} = \tilde{t}_0\left[\frac{\max(T,\xi)}{E_0}\right]^{\beta}. \quad (2.43)$$

Calculation of the infrared renormalisations in the intermediate case $\tilde{t} \sim \xi$, and the system is close to the Anderson localisation threshold is a very difficult mathematical task, but we can assume that in this range of values the renormalisations are of the same nature as in the two limiting cases.

It is moreover reasonable to assume that the infrared renormalisations of a system of defectons localised not because of statistical disorder, but because of strong dissipation, are similar to those discussed above.

We shall now consider the special case of localised defecton states, i.e. we shall consider a two-level system which has been studied on very many occasions.

2.3 Infrared renormalisations for a two-level system

Kondo began his investigations from a two-level system (TLS) in which a quantum defect tunnels between two equivalent equilibrium positions [24]. The expression for the tunnel matrix element is then similar to Eqn (2.28). The dynamics of such a TLS interacting with a dissipative environment has been investigated extensively by the functional integration methods (for a review see Ref. [19]). It has been assumed that the dissipative environment represents a set of independent harmonic oscillators which interact linearly with the TLS. The Hamiltonian of such a 'spin–boson' system is

$$\mathcal{H}_{\rm sb} = -\frac{1}{2}J_0\,\hat{\sigma}_x + \frac{1}{2}\,\xi\,\hat{\sigma}_z + \frac{1}{2}\sum_{\alpha}(m_\alpha\omega_\alpha^2 x_\alpha^2 + p_\alpha^2 m_\alpha^{-1}) + \frac{1}{2}\,a\,\hat{\sigma}_z\sum_{\alpha} C_\alpha x_\alpha, \quad (2.44)$$

where J_0 is the 'bare' splitting of the levels in a TLS as a result of the tunnelling; ξ is the TLS asymmetry; $\tilde{\sigma}_x$ and $\tilde{\sigma}_z$ are the Pauli matrices; the eigenvalue $\sigma_z = \pm 1$ corresponds to a defect localised in the right (left) minimum of the TLS; m_α, x_α, p_α, and ω_α are the mass, coordinate, momentum, and frequency of a given harmonic oscillator; the summation is carried out over all the oscillators; a is the distance between the potential energy minima of the TLS. The quantity C_α describes the coupling between the TLS and an oscillator. It is usual to assume that the environment can be described by a spectral function of the type

$$f(\omega) = \frac{\pi}{2}\sum_{\alpha}\frac{C_\alpha^2}{m_\alpha\omega_\alpha}\,\delta(\omega-\omega_\alpha) = A\,\omega^{s}\mathrm{e}^{-\omega/\omega_{\rm c}}, \quad (2.45)$$

where $A = \text{const}$, $\omega_{\rm c}$ is the limiting frequency of the oscillators, and the power exponent s is selected from physical considerations. In the case of the interaction with phonons in a three-dimensional crystal, we have $\omega_{\rm c} = \theta$, and $s = 5$ or 3, and the tunnelling occurs between crystallographically equivalent or inequivalent interstices, respectively.

It follows from perturbation theory that the interaction of a quantum defect with electrons is equivalent to the interaction with bosons when we have $\omega_{\rm c} = E_0$ and $s = 1$ (Tomonaga bosons) [17]. The case $s = 1$ is known as the ohmic dissipation.

Functional integration with respect to variables of the dissipative environment yields the effective action on a quantum defect, which determines its behaviour.

Calculations show that at $T = 0$ a defect remains localised in one minimum if $s < 1$ and also for $s = 1$, provided the parameter $\beta' = Aa^2/h$ exceeds unity. If $\beta' < 1$, a renormalised tunnel matrix element $J/2$ is given by

$$J = J_0(J_0\,E_0^{-1})^{\beta'/(1-\beta')}. \quad (2.46)$$

However, as shown earlier [25, 26], the above scheme does not allow for the reaction of a TLS on the thermostat, although such neglect is permissible only if $\beta' \ll 1$. The actual localisation of a particle in one of two equivalent minimal finite depths is unlikely even in the strong dissipation case.

We shall now consider the interaction of electrons with two-level systems.

The Hamiltonian of an isolated TLS is

$$\mathcal{H}_{\mathrm{TLS}} = -\frac{\xi}{2}\, c_1^+ c_1 + \frac{\xi}{2}\, c_2^+ c_2 + \frac{J_0}{2}\,(c_1^+ c_2 + c_2^+ c_1)\,, \tag{2.47}$$

where J_0 and ξ are defined above, whereas c_j^+, c_j are the second-quantisation operators for a defecton in the j-th potential well.

The interaction of a TLS with electrons is described by the Hamiltonian

$$\mathcal{H}_{\mathrm{e-TLS}} = \sum_{\boldsymbol{k},\boldsymbol{k}'} V_0(\boldsymbol{k}-\boldsymbol{k}')a^+(\boldsymbol{k}')a(\boldsymbol{k}) \times \exp[\mathrm{i}(\boldsymbol{k}-\boldsymbol{k}')\cdot\boldsymbol{R}_j]c_j^+ c_j\,, \tag{2.48}$$

where $\boldsymbol{R}_j$ are the coordinates of the TLS minima.

After diagonalisation of the Hamiltonian $\mathcal{H}_{\mathrm{TLS}}$ we have

$$\mathcal{H}_{\mathrm{TLS}} = \sum_{j=1,2} (-1)^j\, \frac{E}{2}\, \widetilde{c}_j^+ \widetilde{c}_j\,, \tag{2.49}$$

where

$$E = (\xi^2 + J_0^2)^{1/2}\,,$$
$$\widetilde{c}_1 = \widetilde{a}c_1 - \widetilde{b}c_2,\ \widetilde{c}_2 = \widetilde{a}c_2 + \widetilde{b}c_1,\ \widetilde{a} = [0,5\,(1+\xi E^{-1})]^{1/2}\,,$$
$$\widetilde{b} = [0,5\,(1-\xi E^{-1})]^{1/2}\,. \tag{2.50}$$

In the new basis the Hamiltonian $\mathcal{H}_{\mathrm{e-TLS}}$ becomes

$$\begin{aligned}\mathcal{H}_{\mathrm{e-TLS}} = \sum_{j,\boldsymbol{k},\boldsymbol{k}'} V_0(\boldsymbol{k}-\boldsymbol{k}')a^+(\boldsymbol{k}')a(\boldsymbol{k})\{&\exp[\mathrm{i}(\boldsymbol{k}-\boldsymbol{k}')\cdot\boldsymbol{R}_1] \\ &\times[\widetilde{a}^2\widetilde{c}_1^+\widetilde{c}_1 + \widetilde{b}^2\widetilde{c}_2^+\widetilde{c}_2 + \widetilde{a}\widetilde{b}(\widetilde{c}_2^+\widetilde{c}_1 + \widetilde{c}_1^+\widetilde{c}_2)] \\ &+\exp[\mathrm{i}(\boldsymbol{k}-\boldsymbol{k}')\cdot\boldsymbol{R}_2]\,[\widetilde{a}^2\widetilde{c}_2^+\widetilde{c}_2 + \widetilde{b}^2\widetilde{c}_1^+\widetilde{c}_1 \\ &-\widetilde{a}\widetilde{b}(\widetilde{c}_2^+\widetilde{c}_1 + \widetilde{c}_1^+\widetilde{c}_2)]\}\,.\end{aligned} \tag{2.51}$$

Calculation of the infrared renormalisations of the 'bare' Green function of defectons and of $V_0(\boldsymbol{k})$ for an arbitrary relationship between J_0 and ξ simplifies only in the case when $k_{\mathrm{F}}a \ll 1$ and $\boldsymbol{a} = \boldsymbol{R}_2 - \boldsymbol{R}_1$, when we can assume that $\exp[\mathrm{i}(\boldsymbol{k}-\boldsymbol{k}')\cdot(\boldsymbol{R}_2-\boldsymbol{R}_1)] = 1$. The renormalisation of the Green functions of a defecton, corresponding to two energy levels, and of the diagonal matrix element $V_{jj}(\boldsymbol{q})$ is described by Eqns (2.42) and (2.40), and the difference between m and g (i.e. the quantity β) can be neglected.

If $|1\rangle$ and $|2\rangle$ are understood to be the ψ functions of a defect localised in the left- and right-hand minima of a TLS, respectively, then the order of magnitude of the matrix element is

$$V_{1,2}^{(0)}(\boldsymbol{k}) \sim \widetilde{t}_0 E_0^{-1} V_{1,1}^{(0)}(\boldsymbol{k})\,, \tag{2.52}$$

so that it has been ignored in our calculations of the infrared renormalisations.

Vladar and Zawadowski [27, 28] have shown that allowance for $V_{1,2}^{(0)}(\boldsymbol{k})$ in the 'noncommuting' case, when

$$\begin{aligned}\sum_{\boldsymbol{k}}\{&[V_{1,1}^{(0)}(\boldsymbol{k}-\boldsymbol{k}_1) - V_{2,2}^{(0)}(\boldsymbol{k}-\boldsymbol{k}_1)]V_{1,2}^{(0)}(\boldsymbol{k}_2-\boldsymbol{k}) \\ &-V_{1,2}^{(0)}(\boldsymbol{k}-\boldsymbol{k}_1)\,[V_{1,1}^{(0)}(\boldsymbol{k}_2-\boldsymbol{k}) - V_{2,2}^{(0)}(\boldsymbol{k}_2-\boldsymbol{k})]\} \\ &\times\frac{1-n[\varepsilon(\boldsymbol{k})]}{\omega-\varepsilon(\boldsymbol{k})} \neq 0\,,\end{aligned} \tag{2.53}$$

leads to the appearance of additional infrared divergences, since now in the absence of the translational invariance the diagrams shown in Fig. 4 do not compensate one another fully. This case is similar to the strongly anisotropic Kondo model. Additional renormalisations may become significant at the Kondo temperature

$$T_{\mathrm{K}} = V_0\left(\frac{\varepsilon_0}{E_0}\right)^{0.5+\{1/[2(2g)^{1/2}]\}}\,, \tag{2.54}$$

if it exceeds E.

Since the magnitude of the infrared renormalisations varies with temperature down to $T \sim E$, it follows that when $T_{\mathrm{K}} \ll E$ such additional renormalisation cannot reach the required quantity.

An estimate of T_{K} obtained in Refs. [27, 28] corresponds to the most optimistic selection of the parameters and gives $T_{\mathrm{K}} \sim 1\,\mathrm{K}$, i.e. of the order of E. However, more realistic estimates give $T_{\mathrm{K}} \leqslant 0.1\,\mathrm{E}$.

Therefore, throughout the investigated range these additional renormalisations can be ignored.

3. Clustering of mobile defects in metals

3.1 Long-range part of the defecton–defecton interaction and the existence of bound states

The problem of the interation of hydrogen atoms in a metal matrix has been the subject of many investigations (see, for example, the monograph of Alefeld and Völkl [29]). All these investigations have been concerned with just one type of the long-range interaction between defects, which is the elastic interaction representing an indirect interaction via acoustic phonons. The energy of this interaction is described by the expression

$$W_{\mathrm{elas}}(\boldsymbol{R}) = W(\boldsymbol{b})\Omega R^{-3}\,, \tag{3.1}$$

where $\boldsymbol{R}$ is the distance between the defects, Ω is the unit-cell volume, and $\boldsymbol{b} = \boldsymbol{R}/R$. Depending on the orientation of the vector $\boldsymbol{b}$ relative to the axes of the crystal lattice, $W(\boldsymbol{b})$ can assume both positive or negative values.

The important role played by another long-range interaction, which is the indirect interaction via the Friedel oscillations of the electron density, is pointed out in Ref. [7]. In the case of a spherical Fermi surface the potential energy of this interaction is [30]

$$\widetilde{W}_{\mathrm{el}}(\boldsymbol{R}) = \frac{\Omega N(0)|V_0(2k_{\mathrm{F}})|^2\cos(2k_{\mathrm{F}}R)}{2\pi\widetilde{\varepsilon}^2(2k_{\mathrm{F}},0)R^3}\,, \tag{3.2}$$

where $\widetilde{\varepsilon}(2k_{\mathrm{F}},0)$ is the permittivity.

In dealing with the interaction between defects of different type, we should replace the term $|(V_0(2k_{\mathrm{F}})|^2$ with the term $[V_{0,1}(2k_{\mathrm{F}})V_{0,2}^*(2k_{\mathrm{F}}) + \mathrm{c.c.}]/2$, where the indices 1 and 2 apply to impurities of different types. As a result of the thermal smearing out of the Kohn singularity $\widetilde{\varepsilon}(\boldsymbol{k},0)$the interaction $W_{\mathrm{el}}(\boldsymbol{R})$ falls exponentially over distances $R_0 = d\varepsilon_{\mathrm{F}}/T$, where d is the lattice constant and ε_{F} is the Fermi energy [31]. This effect is unimportant in the range of

low temperatures under discussion. The statistical disorder does not result in exponential damping of $\widetilde{W}_{\rm el}(\boldsymbol{R})$ [32, 33].

The resultant long-range interaction between impurities is given by

$$W(\boldsymbol{R}) = W_{\rm elas}(\boldsymbol{R}) + \widetilde{W}_{\rm el}(\boldsymbol{R}) . \tag{3.3}$$

The value of $W(\boldsymbol{b})$ varies from 1 eV for heavy interstitial impurities, down to 10^{-2} eV for hydrogen in a metal [34]. The quantity $N(0)|V_0(2k_{\rm F})|^2/2\pi\varepsilon^2(2k_{\rm F},0)$ for values of the parameters typical of a metal amounts to $10^{-2}-1$ eV, $\widetilde{W}_{\rm el}(\boldsymbol{R})$ is of the same order of magnitude as $W_{\rm elas}(\boldsymbol{R})$. In the case of substitutional impurities an indirect interaction via the conduction electrons may predominate.

In addition to the interaction of defects with one another, there is also the interaction with the crystal matrix which has minima at the interstices (for interstitial impurities). We shall assume that these minima are sufficiently steep and that the potential of the matrix is much stronger than $W(\boldsymbol{R})$. This makes it possible to ignore the displacements of the equilibrium positions in interstices caused by the action of $W(\boldsymbol{R})$, compared with $\boldsymbol{a}$, and consider the problem of the distribution of a small number of defects between interstices subject to allowance for the pair interaction between the defects [35, 36]. Naturally, in the case when $R \sim d$, we need to allow for the short-range part of the defecton – defecton interaction.

3.2 Clustering of defects

Since $W(\boldsymbol{b})$ and $\widetilde{W}_{\rm el}(\boldsymbol{R})$ can be either positive or negative, there is a set of interstices with $W(\boldsymbol{R}) < 0$ and the state with the lowest energy $-W_0$ corresponds to $R_0 \sim d$ for $k_{\rm F}d \sim 1$. The short-range part of the interaction between defects may alter the sign of the interaction, even in the most unfavourable case, only for several defect positions closest to one another. Therefore, *all* the mobile point defects in a metal and neutral mobile impurities in an insulator should form clusters as a result of cooling [35, 36].

The clustering may result in stratification into phases with high and low defecton concentrations and clusters may form from a finite number of particles.

A typical clustering temperature found from a simple statistical calculation has the following value at low defecton concentrations such that $x \ll 1$:

$$T_{\rm cl} = W_0|\ln x|^{-1} , \tag{3.4}$$

where W_0 is the specific binding energy of defectons in a highly concentrated phase or in a cluster.

The proportion of free (unclusterised) defectons κ is

$$\kappa = \left(1 + \gamma x \exp\frac{W_0}{T}\right)^{-1} , \tag{3.5}$$

where $\gamma \sim 1$ if we assume that there is only one bound state with a specific binding energy W_0 or

$$\kappa = \left[1 + \gamma x \left(\frac{T}{W_0}\right)^2 \exp\frac{W_0}{T}\right]^{-1} , \tag{3.6}$$

if we allow for the presence of a large number of bound defect states [36].

In any case, the value of κ falls exponentially at temperatures $T < T_{\rm cl}$.

In the majority of cases the phase with clusters formed from a finite number of particles is metastable compared with large-scale stratification in the phase with high and low defect concentrations. However, these metastable states occur relatively frequently, since the binding of mobile defects into clusters reduces strongly their mobility and increases the time taken to reach an equilibrium (relaxation time).

The presence of an interaction $\widetilde{W}_{\rm el}(\boldsymbol{R})$ oscillating with the distance in a metal can make the following clustering scenario energetically favourable: at some characteristic temperature $T_{\rm cl.1}$ the clusters form from several particles (quasimolecules), but at lower temperature $T_{\rm cl.2}$ the quasimolecules become clustered. A typical distance between quasimolecules in a growing second-generation cluster is much greater than the distance between defects in a quasimolecule, which is the reason for the low specific binding energy in a cluster compared with the specific binding energy of defects in a quasimolecule (and, consequently, the reason why $T_{\rm cl.2}$ is lower than $T_{\rm cl.1}$). If the number of molecules in a second-generation cluster is also limited, then the next stage of the clustering process begins at a lower temperature $T_{\rm cl.3}$, etc.

The formation of quasimolecules is not a phase transition in the true sense of the word, since this process occurs in a temperature range defined by

$$\Delta T = T_{\rm cl}|\ln x|^{-1} , \tag{3.7}$$

and all the thermodynamic characteristics of the system vary continuously.

Quasimolecules formed from two hydrogen (deuterium) atoms have been observed by the method of diffuse elastic neutron scattering in the hydrides of metals of the third group: LuD_x [37, 38], $YH(D)_x$ [39, 40], ScD_x [41]. The hydrogen isotopes occupy the tetrahedral pores of the hcp matrix of the metal. When a quasimolecule is formed, the second hydrogen atom occupies the second-nearest tetrahedral pore along the hexagonal axis, which is symmetric relative to the nearest site atom (Fig. 8).

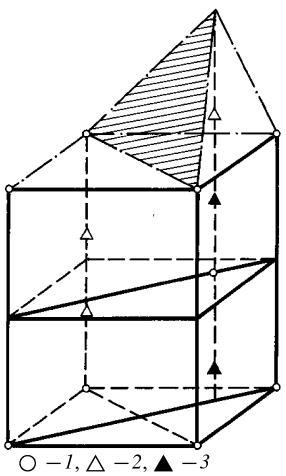

Figure 8. Tetrahedral interstices in the hcp matrix of a metal: (*1*) site atom; (*2*) tetrahedral interstice; (*3*) interstices occupied by the formation of a quasimolecule.

The phase diagram of the hydrides of scandium, yttrium, and some rare-earth elements is shown in Fig. 9 [36]. The fraction of quasimolecules at 400 K is fairly high to prevent splitting into high- and low-concentration phases in the range $x < x_{\rm cr}$ [39]. The value of $x_{\rm cr}$ varies from 0.03 for ErH_x [42] to 0.35 for ScH_x [43]. In the range 150 – 200 K there are

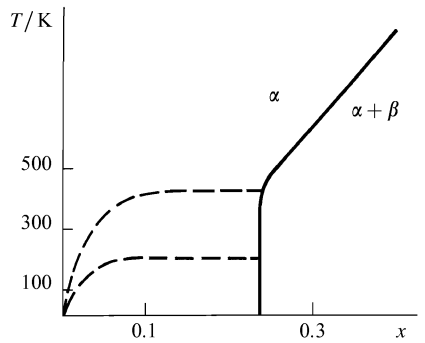

Figure 9. Phase diagram of the hydrides of yttrium, scandium, and some rare-earth elements.

anomalies of the electrical resistivity and specific heat of the hydrides, indicating clustering of quasimolecules [42–45].

Neutron measurements indicate the absence of a long-range order in the phase with a high concentration of the hydrogen pairs. Therefore, the transition from a lattice gas to a lattice liquid occurs in the system of quasimolecules at 150–200 K.

When the concentration of immobile defects exceeds greatly the concentration of mobile defects, the formation of clusters from one immobile and one mobile (or several mobile) impurities becomes possible. Then x in Eqns (3.4)–(3.7) should be replaced with the concentration of immobile defects and W_0 is the binding energy between mobile and immobile defects. The example of such clustering is the capture of hydrogen by O, N, and C atoms in niobium. These atoms occupy octahedral interstices in the bcc lattice of niobium and hydrogen atoms are at tetrahedral interstices. As a result of an interaction with a heavy impurity C, N, or O at $T < 150$ K a hydrogen atom occupies one of two equivalent equilibrium positions corresponding to the two nearest tetra-hedral interstices (Fig. 10) [4]. The tunnelling between these two equilibrium positions gives rise to a two-level system (TLS).

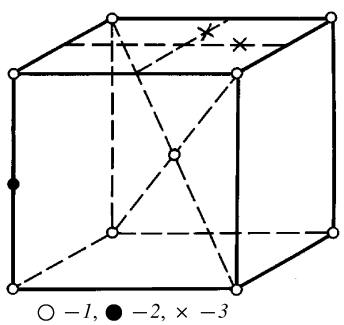

Figure 10. Two-level system in a niobium single crystal: (*1*) niobium atoms; (*2*) atom of a heavy impurity; (*3*) equilibrium positions of the hydrogen atom.

Anomalies of the specific heat associated with such two-level systems were first reported in Ref. [46] and they have since been investigated by measurements of the specific heat [47, 48], thermal conductivity [49], internal friction [50–52], and ultrasonic parameters [53–56]. The fullest information is provided by the inelastic neutron scattering method [57–62].

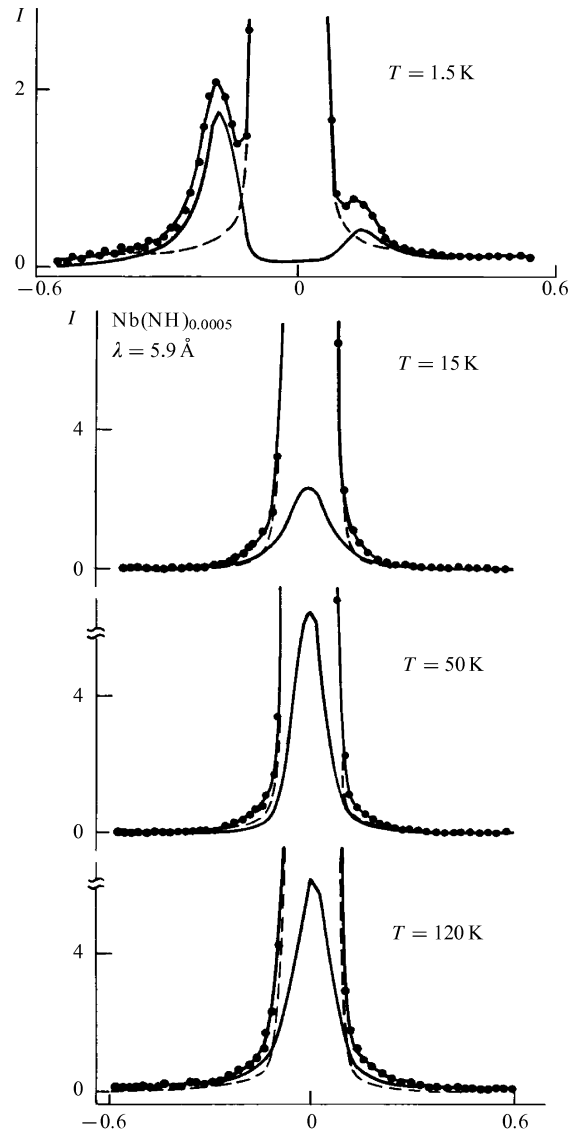

Figure 11. Dependences of the intensity of inelastic neutron scattering in $Nb(NH)_{0.0005}$ on the change in the energy (meV) at different temperatures.

At low temperatures there is a clear side peak in the inelastic scattering intensity (Fig. 11). The results of these measurements give $J = 226 \pm 4$ μeV for $Nb(OH)_x$, $J = 165 \pm 4$ μeV for Nb(NH), and $J = 162 \pm 4$ μeV for $Nb(CH_x)$ [61] and $T \to 0$ in the superconducting phase. The dependence of the value of J on the nature of the heavy impurity is evidence of different strains in the niobium lattice around impurities of different types [62].

In the absence of such strains the width of the free-defecton band in niobium would have been zJ, where z is the number of the nearest equivalent interstices. In the presence of lattice strains this relationship can be used as an order-of-magnitude estimate.

At temperatures $T > 10$ K, when $\tau_d J \ll 1$, instead of a side peak the scattering spectrum has a quasielastic central maximum of width proportional to the frequency of hydrogen jumps between the TLS minima.

The value of J for deuterium captured by a nitrogen impurity has been found as a result of ultrasonic investigations [56] and has proved to be $J = 0.18 \pm 0.01$ K. Similar two-level systems appear also in tantalum, but their

characteristics have been investigated much less thoroughly [46, 63, 64].

The asymmetry of the resultant two-level system is associated with the influence of the remaining systems of this kind and other crystal lattice defects. We shall estimate this asymmetry on the assumption that it is due to the action of 'frozen in' and randomly distributed defects whose concentration is c and that the contribution of mobile defects to the asymmetry is small compared with the contribution of heavy impurities. In the opposite case the collective effects in the system of mobile defects become important.

Since both contributions to the long-range interaction between the defects fall with the distance r between them as r^{-3}, it follows that in the range $c \ll 1$ the distribution of the quantity ξ becomes Lorentzian with the characteristic width δ of the order of

$$\delta = cW(d)\,. \tag{3.8}$$

On the other hand, the scatter of the values of J in a crystal with a low defect concentration ($c \ll 10^{-2}$) can be ignored [65].

An analysis of the data on quasielastic neutron scattering has been used [60, 62] to calculate the frequency $\nu(0)$ of jumps from one interstice to another in the absence of asymmetry. The temperature dependence of this quantity is plotted in Fig. 12 for $Nb(OH)_x$ and $NB(NH)_x$.

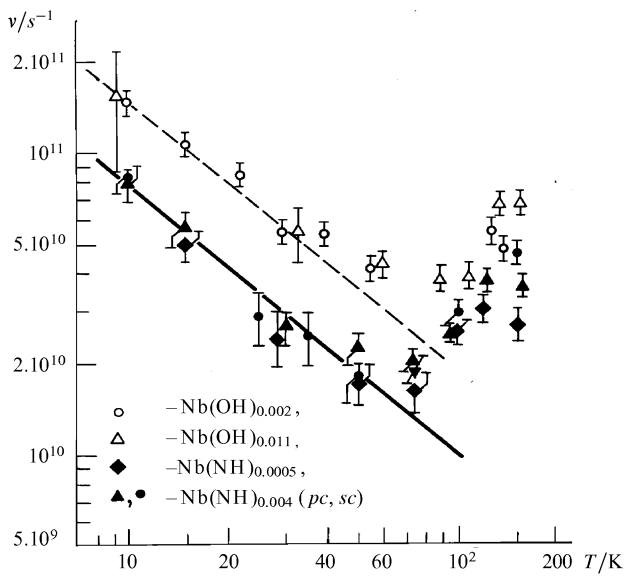

Figure 12. Temperature dependences of the frequency of jumps of hydrogen between minima of two-level systems in $Nb(OH)_x$ and $Nb(NH)_x$; here, *pc* is a polycrystalline sample and *sc* is a single crystal.

Below 60 K the dependence of $\nu(0)$ on T is approximated satisfactorily by the law $\nu(0) \propto T^{-1}$ and a comparison with the expression for the jump frequency

$$\nu(0) = \frac{J^2}{4\pi\beta T\hbar}$$

(see Refs [17, 10]) has made it possible to obtain the value $\beta = 0.055$ for hydrogen in niobium [60]. Moreover, the ratio of the jump frequencies for $Nb(OH)_x$ and $Nb(NH)_x$ is in good agreement with the ratio of the values of J^2 deduced from inelastic neutron scattering.

It follows that below 60 K the quantum diffusion of hydrogen in niobium is governed by the processes of defecton scattering on electrons, whereas below 60 K the interaction with phonons begins to play a significant role.

Two-level systems appear readily also in the hydrides of metals of the third group mentioned above. Unpaired hydrogen atoms are more likely to tunnel to the nearest interstice located on the hexagonal axis (Fig. 8) than to other equiva-lent interstices. There is also some similarity between two-level systems formed by such two interstices. Investigations of scandium hydrides by quasielastic neutron scattering [66, 67] have yielded a curve similar to that shown in Fig. 12. The value of $\tau_d J$ has been compared with unity at 15.7 K and the values of J and β have been found to be 0.32 meV and 0.039, respectively. The high value of J is associated with shorter, com-pared with niobium, distance between the TLS minima. A mini-mum of the jump frequency $\nu(0)$ has been observed at $T = 100$ K.

4. Transport coefficients in metals with quantum defects

4.1 Metal with free defectons

4.1.1 Electrical conductivity

We shall now consider the influence of quantum defects on the electron subsystem of a metal. We shall first investigate the case of free defectons described by the Bloch wave functions. We shall begin with the Hamiltonian of Eqns (2.1), (2.3), and (2.4), used in Section 2.1 to study the infrared renormalisations in an ideal crystal. However, whereas in the case of the infrared renormalisations we have been interested primarily in the defecton Green function, we shall now concentrate our attention on the contribution of defectons to the self-energy part of the electron Green function $\Sigma_1(\boldsymbol{k}, \varepsilon_k)$.

Diagrams of the type shown in Fig. 13a lead only to renormalisation of the chemical potential of electrons and the contribution of defectons to the imaginary part of $\Sigma_1(\boldsymbol{k}, \varepsilon_k)$ considered within the framework of the parquet approximation is described by the diagram shown in Fig. 13b [9, 68] (the notation is the same as in Section 2). It corresponds to the expression

$$\Sigma_{1d}(\boldsymbol{k}, \varepsilon_k) = 2\int \frac{d\boldsymbol{p}\, d\boldsymbol{p}'}{(2\pi)^6} |V_0(\boldsymbol{p}-\boldsymbol{p}')|^2 \left[\frac{\max(T, \varepsilon_0)}{E_0}\right]^g \times \frac{N(\boldsymbol{p}')[1-N(\boldsymbol{p})][1-n(\boldsymbol{k}+\boldsymbol{p}'-\boldsymbol{p})]+N(\boldsymbol{p})[1-N(\boldsymbol{p}')]n(\boldsymbol{k}+\boldsymbol{p}'-\boldsymbol{p})}{i\varepsilon_k-\omega(\boldsymbol{p})+\omega(\boldsymbol{p}')-\varepsilon(\boldsymbol{k}+\boldsymbol{p}'-\boldsymbol{p})+\mu}\,, \tag{4.1}$$

where

$$N(\boldsymbol{p}) = \{\exp[(\tilde{\omega}(\boldsymbol{p}) - \zeta)T^{-1}] + 1\}^{-1} \tag{4.2}$$

is the Fermi distribution function of defectons.

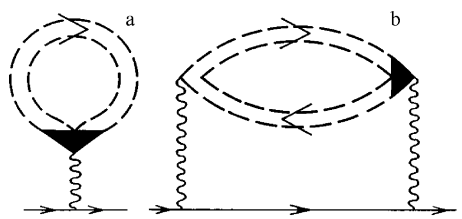

Figure 13. Diagrams for the self-energy part of the electron Green function.

After analytic continuation from the points $\varepsilon = \mathrm{i}\varepsilon_k$ to the real axis, the integration over regions far from the pole of Eqn (4.1) yields a constant renormalisation of μ and a negligibly small (of the order of xg) renormalisation of the defecton path, whereas integration near the pole gives $\operatorname{Im}\Sigma_{1\mathrm{d}}(\boldsymbol{k},\varepsilon)$. On the mass surface the result is

$$\begin{aligned}\operatorname{Im}\Sigma_{1\mathrm{d}}(\boldsymbol{k},\varepsilon) = -\operatorname{sgn}\varepsilon \int \frac{\mathrm{d}\boldsymbol{p}\,\mathrm{d}\boldsymbol{p}'}{(2\pi)^5}\,|V_0(\boldsymbol{p}-\boldsymbol{p}')|^2 \\ \times\left[\frac{\max(T,\varepsilon_0)}{E_0}\right]^g \{N(\boldsymbol{p}')[1-N(\boldsymbol{p})][1-n(\boldsymbol{k}+\boldsymbol{p}'-\boldsymbol{p})] \\ +N(\boldsymbol{p})\,[1-N(\boldsymbol{p}')]\,n(\boldsymbol{k}+\boldsymbol{p}'-\boldsymbol{p})\} \\ \times\delta[\varepsilon(\boldsymbol{k})-\omega(\boldsymbol{p})+\omega(\boldsymbol{p}')-\varepsilon(\boldsymbol{k}+\boldsymbol{p}'-\boldsymbol{p})]\,. \qquad (4.3)\end{aligned}$$

In the temperature range $T \gg \varepsilon_0$, when $\omega(\boldsymbol{p})$ and $\omega(\boldsymbol{p}')$ can be ignored in the argument of the δ function in Eqn (4.3) and we can assume that $N(\boldsymbol{p}) = \mathrm{const} \ll 1$, the corresponding result is

$$\operatorname{Im}\Sigma_{1\mathrm{d}}(\boldsymbol{k},\varepsilon) = -\frac{\operatorname{sgn}\varepsilon}{2\tau_{\mathrm{e,d,st}}}\left(\frac{T}{E_0}\right)^g, \qquad (4.4)$$

where $\tau_{\mathrm{e,d,st}}$ is [1]

$$\tau^{-1}_{\mathrm{e,d,st}}(\boldsymbol{k}) = \frac{x}{\Omega}\int \frac{|V_0(\boldsymbol{k}-\boldsymbol{k}')|^2\,\mathrm{d}\boldsymbol{k}'}{(2\pi)^2|\nabla\varepsilon(\boldsymbol{k}')|}, \qquad (4.5)$$

and integration is carried out over the Fermi surface.

The rate of relaxation of electrons, governed by their scattering of defectons, is $\tau^{-1}_{\mathrm{e,d}}$ and it differs from the corresponding value $\tau^{-1}_{\mathrm{e,d,st}}$ in the case of scattering of electrons by randomly distributed 'frozen-in' (static) defects of the same chemical nature: the difference is a factor of $(T/E_0)^g$.

In exactly the same way we can show that if $T \gg \widetilde{\varepsilon}_0$, such a relationship applies also to the electron transport time governed by the scattering of defectons, i.e. when $T \gg \widetilde{\varepsilon}_0$ the contribution of the scattering by defectons to the electrical resistivity is

$$\rho = \rho_0(TE_0^{-1})^g, \qquad (4.6)$$

where ρ_0 is the residual resistivity in the case of randomly distributed 'frozen-in' impurities of the same chemical nature [9, 68].

Kondo [69] has attempted to calculate the contribution of quantum defects to the resistivity of metal. The renormalisation of the defecton Green functions has been ignored and the replacement of the 'bare' vertex of the electron–defecton interaction with the complete vertex has been carried out for both vertices in Fig. 13b. The result is an increase in the resistivity when the temperature is lower in accordance with the law $\rho = \rho_0(E_0/T)^{2g}$.

The fall of the resistivity with the fall in temperature is natural, since an increasing proportion of electrons can match adiabatically the motion of defectons. In fact, at $T = 0$ the nonadiabatic behaviour is exhibited by electrons which are in a narrow belt of width $\widetilde{\varepsilon}_0$ near the Fermi surface. These electrons are not sufficiently fast to match the defecton motion. As the temperature is increased, the appearance of electronic excitations makes the width of this belt of the order of T.

We must make two important methodological comments before we consider low temperatures. At first sight it seems essential to review the results of calculations of the infrared renormalisations allowing for $\operatorname{Im}\Sigma_{1\mathrm{d}}(\boldsymbol{k},\varepsilon)$. However, this cannot be done because ladder-type corrections to the

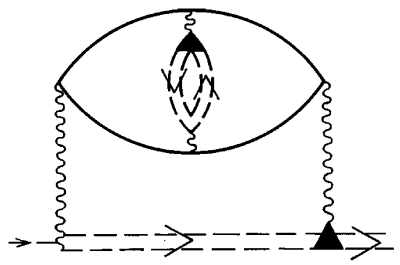

Figure 14. Corrections to the vertex compensating for the damping of the electron Green function.

electron–defecton vertex $V_0(\boldsymbol{q})$ containing new defecton loops (Fig. 14) compensate for the appearance of the self-energy part $\Sigma_{1\mathrm{d}}$ in the electron Green function and the expression for the electron loop is not affected.

The second comment refers to going over to the limit $\varepsilon_0 \to 0$. We can see that Eqn (4.6) does not contain the tunnelling matrix element (width of the defecton band) which characterises the quantum properties of a defect. Therefore, the same temperature dependence of the resistivity should be observed also for a metal with heavy thermalised defects. In other words, in the limit $\varepsilon_0 \to 0$ the results of our analysis do not agree with those obtained by the 'cross' technique [1]. This is because in this technique the 'frozen-in' impurities as regarded are an external field acting on electrons and we consider them to be the internal degrees of freedom of a crystal and we deal with the scattering of electrons by an equilibrium system of defects. However, the relaxation time t_0 of the defecton subsystem is governed by the value ε_0 and it increases exponentially with increase in the mass defect. Measurements are, however, made after a considerable time $t \gg T_0$ after a change in temperature, which in reality requires a very long wait. Therefore, at the usual rates of measurements the system of heavy defects cannot reach an equilibrium and it can be regarded as 'frozen-in'. The presence of these 'frozen-in' defects in a real sample gives rise to a residual resistivity. When the concentration of 'frozen-in' defects is $c \gg x$ the temperature-dependent contribution of defectons can easily be separated from the background of this residual resistivity.

We shall now turn back to the contribution of defectons to the electrical resistivity at temperatures $T \ll \widetilde{\varepsilon}_0$. In the case of an open Fermi surface it follows readily from Eqn (4.3) that the relaxation time of electrons due to their scattering by defectons is inversely proportional to temperature, $\tau_{\mathrm{e,d}} \propto T^{-1}$, since the electron momentum now changes as a result of the scattering by an amount of the order of the thermal momentum $\widetilde{k}$ of a defecton, which reduces the phase volume of the final states of an electron by the factor $(\widetilde{k}/k_{\mathrm{F}})^2$. The contribution of defectons to the resistivity is of the order of [9]

$$\rho = \rho_0\left(\frac{\varepsilon_0}{E_0}\right)^g\left(\frac{T}{\widetilde{\varepsilon}_0}\right)^2, \qquad (4.7)$$

since ρ includes the transport scattering time and the factor $(1-\cos\varphi)$, where φ is the angle of the scattering of an electron by a defecton, contributes an additional smallness of the $(\widetilde{k}/k_{\mathrm{F}})^2 \sim T/\widetilde{\varepsilon}_0$ type. As before, we are assuming that $k_{\mathrm{F}} \sim k_{\mathrm{B}}$. In the case of a closed Fermi surface the resistivity ρ, like that for the scattering by phonons, falls exponentially with temperature, although not at $T < \theta$ but at $T < \widetilde{\varepsilon}_0$. In

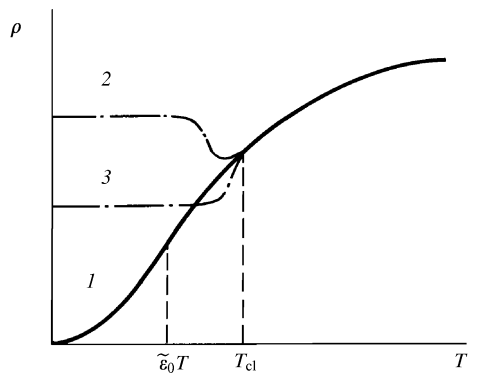

Figure 15. Temperature dependence of the defecton contribution to the resistivity: (*1*) in the absence of clustering; (*2*, *3*) after allowing for clustering.

accordance with our hypothesis, the defecton gas still remains nondegenerate.

A typical temperature dependence $\rho(T)$ is shown in Fig. 15.

We have ignored so far the process of defecton clustering. If the concentration of heavy immobile impurities is $c \ll x$, either separation into phases with high and low defecton concentrations takes place or clusters with a finite number of particles are formed. When a multiphase system is formed, the transport coefficients of a metal depend on the dimensions of single-phase regions and on their configuration. The thermo-dynamic equilibrium of a crystal at $T \to 0$ corresponds to the existence of an ultrapure phase and a phase with a high con-centration of impurities (distributed in an ordered manner) in the form of two domains, but the establishment of such a state requires an enormous time on the geological scale.

When clusters form from a finite number of defectons, their mobility can be ignored, i.e. we can regard as 'frozen-in' that fraction of defects which forms clusters. In this case the relaxation time of electrons $\tau_{e,\,imp}$ is

$$\tau_{e,\,imp}^{-1}(T) = \kappa(T)\tau_{e,\,d}^{-1}(T) + [1 - \kappa(T)]\tau_{e,\,cl}^{-1}\,, \tag{4.8}$$

where the dependence $\kappa(T)$ is given by Eqn (3.6) and the time $\tau_{e,\,d}$ corresponds to the scattering by defects which have not formed clusters ($\kappa = 1$) and the time $\tau_{e,\,cl}$ corresponds to the scattering on 'frozen-in' clusters when $\kappa = 0$.

It follows from Eqn (4.8) that at $T < T_{cl}$ the values of $\tau_{e,\,imp}^{-1}(T)$ and, consequently, $\rho(T)$ become constant and are governed by the nature of the clusters that are formed. In the region of T_{cl} either a rise or a fall of $\rho(T)$ may take place (see Fig. 15).

In exactly the same way Eqn (4.8) describes the case of capture of defectons by immobile defects when the concentration is $c \gg x$.

We shall conclude by considering the temperature range in which it should be possible to observe the temperature dependences of the resistivity found above. First, this is the range $T \ll \theta$ where the impurity scattering plays a significant role. However, on the low-temperature side this range is limited by the value T_{cl} which for $x \sim 10^{-2} - 10^{-3}$ amounts to tens or hundreds of kelvin. If the specific binding energy of defects with one another is low, there is a range $10\,\mathrm{K} < T < 100\,\mathrm{K}$ in which the nontrivial dependence $\rho(T)$ should be observed because the defecton contribution to the resistivity is comparable with the phonon contribution. In fact, the order of magnitude is $\tau_{e,\,d,\,tr}^{-1} = xE_0^{1-g}T^g$ and the characteristic relaxation rate of electrons due to their interaction with phonons, $\tau_{e,\,ph,\,tr}^{-1}$, can be estimated as $\tau_{e,\,ph,\,tr}^{-1} \sim 0.1T$ in the range where the dependence $\tau_{e,\,ph,\,tr}^{-1} \propto T$ becomes the dependence $\tau_{e,\,ph,\,tr}^{-1} \propto T^5$ [70]. We can easily see that for $x \approx 10^{-3}$, $g \approx 0.3$, $E_0 \approx 3 \times 10^4\,\mathrm{K}$, $T \approx 30\,\mathrm{K}$, the value of $\tau_{e,\,d,\,tr}^{-1}$ is of the order of $\tau_{e,\,ph,\,tr}^{-1}$.

4.1.2 Thermal conductivity

It is natural to expect a considerable contribution of the scattering by defectons to electron relaxation to result in nontrivial temperature dependences also of other transport coefficients of a metal in the same temperature range. The thermal conductivity of a crystal includes contributions of the electron, phonon, and defecton subsystems which interact with one another.

It has been shown [71] that in the range $T \ll \theta$ the transport of heat is mediated primarily by electrons, exactly as in the case of metals with 'frozen-in' impurities. Since a change in the electron energy due to the scattering by a defecton does not exceed $\tilde{\varepsilon}_0$, it follows that at $T \gg \tilde{\varepsilon}_0$ the scattering is practically elastic. In this range of temperatures the Wiedemann–Franz law is obeyed [70] and the electron contribution to the thermal conductivity is

$$\kappa_e = \frac{\pi^2 T}{3e^2}\,\rho^{-1} = \frac{\pi^2 T}{3e^2\rho_0}\left(\frac{E_0}{T}\right)^g. \tag{4.9}$$

The order of magnitude is

$$\kappa_e = T(xgd)^{-1}\,(E_0 T^{-1})^g \propto T^{1-g}\,. \tag{4.10}$$

At temperatures $T < \tilde{\varepsilon}_0$ the Wiedemann–Franz law is disobeyed because the scattering of electrons by defectons becomes inelastic. The energy relaxation time $\tau_{e,\,d}$ is then

$$\tau_{e,\,d} = \tilde{\varepsilon}_0(TxgE_0)^{-1}\,(E_0\,\varepsilon_0^{-1})^g\,. \tag{4.11}$$

Therefore, at $T \ll \tilde{\varepsilon}_0$, we have

$$\kappa_e = \tilde{\varepsilon}_0\,(xgd)^{-1}\,(E_0\,\varepsilon_0^{-1})^g = \mathrm{const}\,. \tag{4.12}$$

Since $\tau_{e,\,d}$ increases as a result of cooling, at some temperature $T < \tilde{\varepsilon}_0$ it becomes equal to the relaxation time of electrons governed by their scattering on static heavy defects which are always present in a real crystal. Below this temperature the main role is played specifically by such scattering and we have $\kappa_e(T) \propto T$.

In fact, the clustering of defectons begins at $T_{cl} > \tilde{\varepsilon}_0$ and this results in their effective 'freezing' and then the rate of

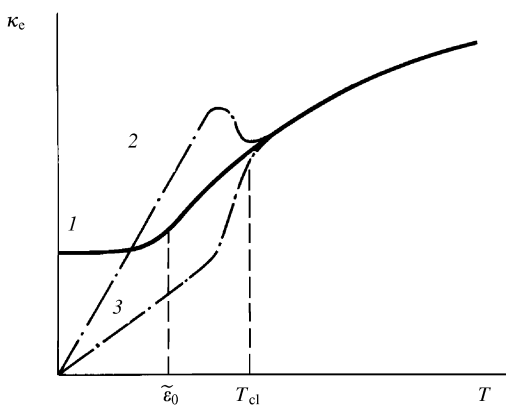

Figure 16. Temperature dependences of the thermal conductivity of a metal with thermalised defects: (*1*) in the absence of clustering; (*2*, *3*) allowing for clustering.

relaxation of electrons assumes a constant value $\tau_{e,cl}^{-1}$ at $T < T_{cl}$ [see Eqn (4.8)]. In this case the order-of-magnitude expression is

$$\kappa = TE_0\tau_{e,\,cl}\,d^{-1} \propto T.$$

Depending on the type of cluster, we can expect a rise or a fall of κ_e at T_{cl} (Fig. 16).

4.1.3 Absorption of sound by electrons

It is well known that at low frequencies when the wavelength of sound λ_s is much greater than the mean free path of electrons l_e the coefficient α_e describing the absorption of sound by electrons is directly proprotional to the electron relaxation time [72–74]. A more careful analysis shows that the quantity α_e is proportional to the time τ_{2e} which differs from the usual relaxation time by the factor $[1 - P_2(\cos\varphi)]$ when integration is carried out over the scattering angle φ, and $P_2(y)$ is a Legendre polynomial [75]:

$$\alpha_e = \frac{n\varepsilon_F\,\omega^2\tau_{2e}}{s^3\rho^*}, \tag{4.13}$$

where n is the electron density; ε_F is the Fermi energy of electrons; ω and s are the frequency and velocity of an acoustic wave; ρ is the density of the metal.

At temperatures $T \ll \theta$ the defect contribution to τ_{2e} predominates for $x \approx 10^{-3} - 10^{-2}$. When the scattering is on static defects, the relaxation time is $\tau_{2e} = \text{const}$ and the temperature dependence of the absorption of sound is related solely to the small contribution made to the relaxation processes related to the electron–phonon and electron–electron interactions.

If the scattering is on mobile defects, the temperature dependence of α_e is due to the temperature dependence of $\tau_{2e,\,d}$ [76]. In the range $T \gg \tilde{\varepsilon}_0$ the main contribution to $\tau_{2e,\,d}^{-1}$ comes from the scattering through large angles and the time $\tau_{2e,\,d}$ differs from $\tau_{e,\,d}$ only by a numerical factor of the order of unity. Therefore, the absorption coefficient of sound obeys the following temperature dependence

$$\alpha_e = \alpha_0(E_0\,T^{-1})^g, \tag{4.14}$$

where α_0 is the absorption coefficient of sound in the case of 'frozen-in' defects.

In the range $T \ll \tilde{\varepsilon}_0$ the main role is played by the low-angle scattering and we have $\tau_{2e,\,d}^{-1} = 3\tau_{e,\,d,\,tr}^{-1}$, where the transport scattering time of electrons $\tau_{e,\,d,\,tr}$ is given by the following order-of-magnitude expression in the case of an open Fermi surface:

$$\tau_{e,\,d,\,tr} = \tau_{e,\,d,\,st}\left(\frac{E_0}{\varepsilon_0}\right)^g\left(\frac{\tilde{\varepsilon}_0}{T}\right)^2. \tag{4.15}$$

Consequently, we have

$$\alpha_e = \alpha_0\left(\frac{E_0}{\varepsilon_0}\right)^g\left(\frac{\tilde{\varepsilon}_0}{T}\right)^2. \tag{4.16}$$

Even in the absence of clustering and heavy immobile defects such a dependence is not observed right down to absolute zero, but only to a certain finite temperature at which the inequality $\lambda_s \gg l_e$ breaks down. If $\lambda_s \ll l_e$, the value of α_e is completely independent of τ_{2e} [72–74]. Therefore, below this temperature the coefficient α_e should assume a constant value. However, as pointed out already, this occurs earlier because of the clustering of defects at T_{cl}. Below T_{cl}, the coefficient α_e reaches a constant value which depends on the nature of the clusters that form. The dependence $\alpha_e(T)$ is plotted in Fig. 17.

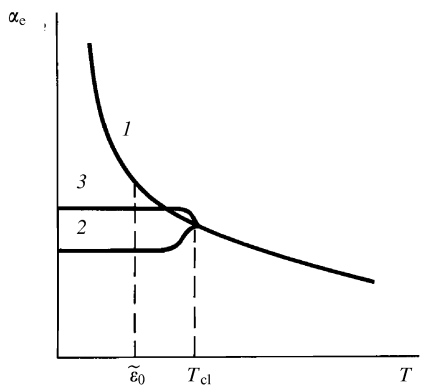

Figure 17. Temperature dependence of the absorption of sound in metals with quantum defects: (*1*) in the absence of clustering; (*2*, *3*) after allowing for clustering.

In addition to the absorption mechanism investigated above, crystals with quantum defects may exhibit a relaxation mechanism of the absorption of sound, but this mechanism is outside the scope of the present review.

4.2 Metal with localised defecton states

We shall now study the nature of the change in our results as we go over from the defecton states described by the Bloch wave functions to localised states. We shall do this by discussing the case when the statistical scatter ξ of the energies of defectons in adjacent interstices, due to an inhomogeneity of the crystal, exceeds greatly $\tilde{\varepsilon}_0$, i.e. when the states of a defecton can be regarded with a high degree of accuracy as localised in a given interstice. This disorder is weak in the electron subsystem ($\xi \ll E_0$) and the conduction electrons are described by the Bloch wave functions [22, 23]. The infrared renormalisations applicable to this case are considered in Section 2.2 on the basis of the Hamiltonian of Eqns (2.35)–(2.37).

In the case considered earlier, when a defecton is described by a Bloch wave function, diagrams of the type shown in Fig. 13a make no contribution to the electron damping. In the present case, i.e. when there are localised defecton states, the scattering process shown in this figure alters the electron momentum. Its contribution is

$$G_0(\boldsymbol{k},\varepsilon_k)G(\boldsymbol{k}',\varepsilon_k)\sum_{\boldsymbol{n}} N(\boldsymbol{n})V_{\boldsymbol{n},\boldsymbol{n}}^{(0)}(\boldsymbol{k}-\boldsymbol{k}')\exp[\mathrm{i}(\boldsymbol{k}-\boldsymbol{k}')\cdot\boldsymbol{R}_{\boldsymbol{n}}]\,, \tag{4.17}$$

where $N(\boldsymbol{n})$ is the Fermi distribution function of defectons in localised states. The renormalisation of the vertex of the electron–defecton interaction of Eqn (2.40) compensates for the renormalisation of the defecton Green function of Eqn (2.42).

We can readily see that, with the exception of the factor $N(\boldsymbol{n})$, Eqn (4.17) is identical with the equation obtained for the scattering of electrons by 'frozen-in' impurities considered by the 'cross' techniques [1]. In the latter case the summation is carried out over impurities.

If we assume that the deviations of $W(\boldsymbol{n})$ from the average value at different interstices are not correlated, the averaging over realisations of the statistical disordering is carried out by analogy with the averaging in the 'cross' technique. Within

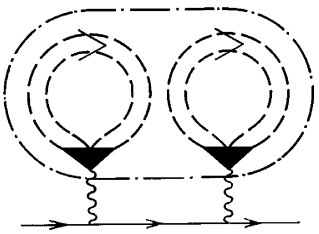

Figure 18. Additional contribution to the damping of electrons which appears in the case of localisation of defecton states.

the framework of our approximation, the contribution of diagrams of this type to the electron damping is described by the diagram in Fig. 18. The chain oval shows that all the defecton loops surrounded by it belong to the same $|\boldsymbol{n}\rangle$.

The second contribution to the damping of electrons is due to the processes described by the diagram in Fig. 13b. In addition to the elastic processes, when both defecton Green functions in a loop correspond to the same $\boldsymbol{n}$, a contribution to the electron damping comes also from the inelastic processes for which the defecton Green function corresponds to different $\boldsymbol{n}$. The contribution of the inelastic processes is small in accordance with the parameter $(\tilde{t}/\xi)^2$. If we ignore this contribution, we find that the expression for $\tau_{\mathrm{e,d}}^{-1}$ is

$$\tau_{\mathrm{e,d}}^{-1}(\boldsymbol{k}) = \sum_{\boldsymbol{n}} \int \frac{|V_{\boldsymbol{n},\boldsymbol{n}}^{(0)}(\boldsymbol{k}-\boldsymbol{k}')|^2 \, \mathrm{d}\boldsymbol{k}'}{\Omega(2\pi)^2 |\nabla \varepsilon(\boldsymbol{k}')|} \{N^2(\boldsymbol{n}) + N(\boldsymbol{n})[1 - N(\boldsymbol{n})](TE_0^{-1})^g\}, \tag{4.18}$$

where integration is carried out over the Fermi surface.

If $V_{\boldsymbol{n},\boldsymbol{n}}^{(0)}(\boldsymbol{k})$ for different interstices are quite similar, so that the differences between them can be ignored, the expression for $\tau_{\mathrm{e,d}}$ assumes its simplest form

$$\tau_{\mathrm{e,d}}^{-1} = \tau_{\mathrm{e,d,st}}^{-1} x^{-1} \sum_{\boldsymbol{n}} \{N^2(\boldsymbol{n}) + N(\boldsymbol{n})[1 - N(\boldsymbol{n})](TE_0^{-1})^g\}. \tag{4.19}$$

In exactly the same way we find that the transport electron time and the resistivity are related by [22, 23]

$$\rho = \rho_0 x^{-1} \sum_{\boldsymbol{n}} \{N^2(\boldsymbol{n}) + N(\boldsymbol{n})[1 - N(\boldsymbol{n})](TE_0^{-1})^g\}. \tag{4.20}$$

If the temperature of a metal is sufficiently high and the occupation numbers $N(\boldsymbol{n})$ are so small that

$$\sum_{\boldsymbol{n}} N^2(\boldsymbol{n}) \ll x(TE_0^{-1})^g, \tag{4.21}$$

the transport coefficients are described by Eqns (4.6), (4.9), and (4.14) obtained in the preceding sections in the absence of diagonal disorder. This is evidence of the universal validity of this temperature dependence and is the main result of the present section.

Subsequent behaviour of the transport coefficients as the temperature is lowered will be considered by taking the example of the contribution of quantum defects to the resistivity. At $T = T'_{\min}$ there is a reversal of the sign of the inequality (4.21). Further cooling is then accompanied by an increase in the resistivity which continues down to the temperature T_{d} of degeneracy of the defecton gas. At $T \ll T_{\mathrm{d}}$ the resistivity is $\rho = \rho_0$. A typical temperature dependence of the resistivity $\rho(T)$

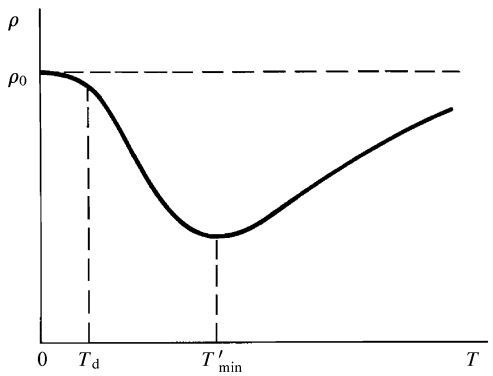

Figure 19. Temperature dependence of the defecton contribution to the resistivity in the presence of disorder.

is plotted in Fig. 19. The values of $T'_{\min}$ and T_{d} are determined by the nature of the density-of-states function $\nu[W(\boldsymbol{n})]$.

Since in a real crystal the disorder is created by crystal lattice defects, the fact that cooling causes the probability of occupancy of the deep defecton levels to approach unity corresponds to the capture (clustering) of defectons by these lattice defects. The equality $\rho(0) = \rho_0$ is a consequence of the model representation of the nature of disorder.

Moreover, the relaxation time of the defecton subsystem rises strongly at $T < T'_{\min}$ because the probability of the excitation of a defect from a deep level falls exponentially with temperature. In a real experiment the defecton system is shown to be 'frozen-in' at low temperatures.

It therefore follows that the behaviour of the transport coefficients of a metal with localised defecton states does not differ from the behaviour in the case of free defecton states.

4.3 Metal with two-level systems

It is clear from the foregoing discussion that the clustering of defectons, leading to their 'freezing' prevents the observation of nontrivial temperature dependences of the transport coefficients of a metal containing quantum defects. In Section 3 we have considered the situation when the capture of a defecton by an immobile heavy impurity creates two-level states. A quantum defect frequently remains mobile also below the clustering temperature. It is therefore natural to expect to observe in this case nontrivial temperature dependences of the transport coefficients even at $T < T_{\mathrm{cl}}$.

We shall consider the contribution of two-level systems to the transport coefficients of a metal on the basis of the formalism developed in Section 2.3 [77]. This contribution is still described by the diagrams in Figs 13b and 18. If the two Green functions in a defecton loop shown in Fig. 13b correspond to states of different energy, the corresponding inelastic contribution to the resistivity contains an additional small term $(k_{\mathrm{F}}a)^2$, which should be compared with the elastic contribution (when both Green functions correspond to the same state), and the inelastic contribution can be ignored.

By analogy with Eqns (4.18)–(4.20), we now obtain the following expression accurate to within terms of the order of $(k_{\mathrm{F}}a)^2$:

$$\tau_{\mathrm{e,d}}^{-1}(\boldsymbol{k}) = \sum_{m} \int \frac{\mathrm{d}\boldsymbol{k}' |V_0(\boldsymbol{k}-\boldsymbol{k}')|^2}{\Omega(2\pi)^2 |\nabla\varepsilon(\boldsymbol{k}')|} \times [1 + 2N_m(1 - N_m)(TE_0^{-1})^g], \tag{4.22}$$

$$\rho = \rho_0 \left[1 + \frac{2\Omega}{x_{\mathrm{TLS}} v} \sum_m N_m (1 - N_m) \, (T E_0^{-1})^g \right], \qquad (4.23)$$

where v is the volume of the system and N_m is the population of the lowest level of the m-th TLS

$$N_m = \frac{\exp(E_m T^{-1})}{\exp(E_m T^{-1}) + 1}. \qquad (4.24)$$

We have ignored here the contribution made to the scattering of electrons by immobile heavy impurities. In addition to their additive contribution to $\tau_{\mathrm{e,d}}$ and ρ, there is also an interference contribution to the scattering shown in Fig. 20. The cross in this figure corresponds to the scattering by an immobile defect and the chain oval shows that the quantum and immobile defects belong to the same TLS. This contribution is independent of temperature and it alters the constant component of ρ.

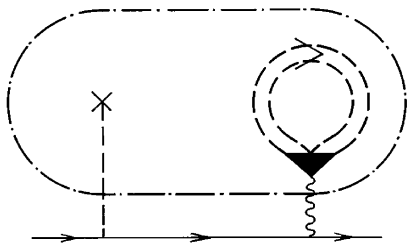

Figure 20. Interference contribution of two-level states to the self-energy part of the electron Green function.

We shall now find the coefficient in front of $(T/E_0)^g$ on the assumption that the distributon of ξ is Lorentzian. If $\delta \gg J_0$, then

$$\begin{aligned} \frac{\Omega}{x_{\mathrm{TLS}} v} \sum_m N_m (1 - N_m) &= \langle N(1-N) \rangle \\ &= \frac{\delta}{4\pi} \int \frac{\mathrm{d}\xi}{\xi^2 + \delta^2} \{\cosh[(\xi^2 + J_0^2)^{1/2} (2T^{-1})]\}^{-2} \\ &= 0.25, \; T \gg \delta, \\ &= T (\pi\delta)^{-1}, \; \delta \gg T \gg J_0 , \\ &= (2 J_0 T \pi^{-1})^{1/2} \delta^{-1} \exp(-J_0 T^{-1}) , \; J_0 \gg T \; ; \end{aligned} \qquad (4.25)$$

here $\langle \ldots \rangle$ denotes the averaging of two-level systems.

If $J_0 \gg \delta$, then

$$\begin{aligned} &\langle N(1-N) \rangle \\ &= 0.25 \{\cosh[J_0 (2T)^{-1}]\}^{-2}, \; T \gg \delta^2 (2J_0)^{-1}, \\ &= (2 J_0 T \pi^{-1})^{1/2} \delta^{-1} \exp(-J_0 T^{-1}), \; \delta^2 (2J_0)^{-1} \gg T . \end{aligned} \qquad (4.26)$$

It therefore follows that in the range $T_{\mathrm{cl}} \gg T \gg \max(\delta, J_0)$ the dependence $\tau_{\mathrm{e,d}}^{-1} = A + B(T/R_0)^g$ is obeyed by $\tau_{\mathrm{e,d}}$; here, A and B are constants of the same order of magnitude. Since at temperatures much below the Debye value the contribution of two-level systems to the rate of relaxation of electrons is the dominant one, such a dependence of $\tau_{\mathrm{e,d}}$ leads to anomalous temperature dependences of the transport coefficients of a metal containing two-level systems.

In particular, the contribution of these systems to the resistivity is

$$\rho = \rho_{\mathrm{st}} + \rho_0 [1 + 0.5 \, (T E_0^{-1})^g], \qquad (4.27)$$

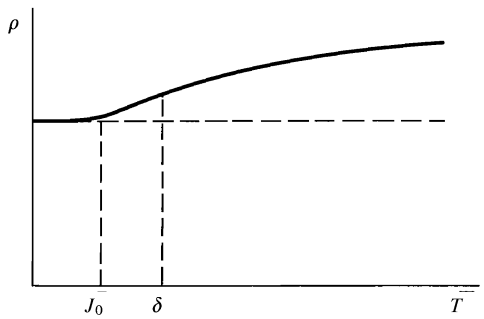

Figure 21. Temperature dependence of the contribution of two-level systems to the resistivity.

where ρ_{st} is the contribution to the static (immobile) defects and the interference contribution to the resistivity. The temperature dependence of ρ is plotted in Fig. 21. For $g \sim 0.3$, $E_0 \sim 3 \times 10^4$ K, and $T \sim 30$ K the temperature-dependent term in ρ amounts to just a few percent.

It would undoubtedly be of interest to investigate experimentally the temperature dependences of the resistivity of the compounds $\mathrm{Nb(OH)}_x$, $\mathrm{Nb(NH)}_x$, and $\mathrm{Nb(CH)}_x$.

5. Summary

We shall now formulate our conclusions and proposals.

5.1 Conclusions

1. The interaction of defectons with electrons leads to major infrared renormalisations of the defecton Green function and of the vertex of the electron–defecton interaction. The renormalised quantities acquire an additional temperature dependence of the T^g type, where g depends on the properties of a given material, i.e. it is not universal.

2. The interaction with electrons gives rise to an electron cloud around a defect (electron polaron effect). This results in an additional narrowing of the defecton band and this narrowing depends on temperature as T^β. In the case of localised defecton states the electron polaron effect reduces the probability of a transition to an adjacent interstice.

3. The long-range part of the interaction between defects in the matrix of a metal is due to both the elastic interaction and the indirect interaction mediated by the Friedel oscillations of the electron density. In the case of light interstitial impurities this indirect interaction may be of the same order of magnitude as the elastic interaction between defects.

4. Since these two interactions can have either sign, a large number of bound defect states appears irrespective of the nature of the short-range interaction between defects. When temperature is lowered the unavoidable effect is the clustering of all mobile defects in a metal and of neutral mobile impurities in an insulator. The final result is either separation into phases with high and low defect concentrations or the appearance of clusters made up from a finite number of particles.

5. The formation of clusters reduces strongly the defect mobility and this in turn prevents the attainment of a thermodynamic-equilibrium state. Consequently, instead of impurity clusters with a large number of particles, only small clusters consisting of two or three particles are formed.

6. At temperatures $T_{cl} < T < \theta$ the main electron relaxation mechanism in metals with quantum defects is the scattering of electrons by defects.

7. The infrared renormalisations due to the electron–defecton interaction lead to nontrivial temperature dependences of the rate of relaxation of the electron subsystem and, consequently, of the transport coefficients of a metal, including the electron contribution to the absorption coefficient of sound.

8. The clustering of defects hinders the appearance of such dependences and reduces the range of temperatures in which they are observed.

9. Nontrivial temperature dependences of the transport coefficients of a metal may be observed also at $T < T_{cl}$ if the capture of defectons by heavy immobile defects gives rise to two-level systems.

10. The distribution of the asymmetry of such two-level systems is Lorentzian with a characteristic width proportional to the defect concentration. The scatter of the values of the tunnel matrix element of two-level systems in a crystal with a low defect concentration ($c \sim 10^{-2}$) can be ignored.

5.2 Proposals

Unfortunately, in the literature we have reviewed there are no reports of experimental investigations of the temperature dependences of the transport coefficients of dilute hydrides of metals ($x \sim 0.1 - 1\%$) at low temperatures.

On the basis of the theory proposed above it would be of great interest to investigate such dependences for single-phase (in respect of composition) dilute metal hydrides with a low temperature of splitting into phases with high and low hydrogen concentrations.

Moreover, it would be very desirable to carry out investigations of the transport coefficients of niobium and tantalum crystals, which contain two-level systems, and to search and study similar two-level systems in other metals.

Acknowledgement

We are grateful to A P Zhernov for valuable discussions.

References

1. Abrikosov A A, Gorkov L P, Dzyaloshinskii I E *Methods of Quantum Field Theory in Statistical Physics* (Englewood Cliffs, NJ: Prentice-Hall, 1963)
2. Kondo J *Physica B (Utrecht)* **123** 175 (1984)
3. Andreev A F, Lifshitz I M *Zh. Eksp. Teor. Fiz.* **56** 2057 (1969) [*Sov. Phys. JETP* **29** 1107 (1969)]
4. Magerl A, Rush J J, Rowe J M, et al. *Phys. Rev. B* **27** 927 (1983)
5. Zaitzev R O, Malkin I A *Fiz. Nizk. Temp.* **2** 69 (1976) [*Sov. J. Low Temp. Phys.* **2** 35 (1976)]
6. Zyryanov P S, Klinger M I *Kvantovaya Teoriya Yavlenii Elektronnogo Perenosa v Kristallicheskikh Poluprovodnikakh* (Quantum Theory of Electron Transport Phenomena in Crystalline Semiconductors) (Moscow: Nauka, 1976)
7. Morosov A I *Zh. Eksp. Teor. Fiz.* **77** 1471 (1979) [*Sov. Phys. JETP* **50** 738 (1979)]
8. Yu C C, Granato A V *Phys. Rev. B* **32** 4793 (1985)
9. Morozov A I, Sigov A S *Fiz. Nizk. Temp.* **13** 606 (1987) [*Sov. J. Low Temp. Phys.* **13** 341 (1987)]
10. Kagan Yu, Prokof'ev N V *Zh. Eksp. Teor. Fiz.* **90** 2176 (1986) [*Sov. Phys. JETP* **63** 1276 (1986)]
11. Kondo J, Soda T *J Low Temp. Phys.* **50** 21 (1983)
12. Roulet B, Gavoret J, Nozieres P *Phys. Rev.* **178** 1072 (1969)
13. Nozieres P, Gavoret J, Roulet B *Phys. Rev.* **178** 1084 (1969)
14. Nozieres P, De Dominicis C T *Phys. Rev.* **178** 1097 (1969)
15. Yamada K *Progr. Theor. Phys.* **75** 1044 (1986)
16. Anderson P W *Phys. Rev. Lett.* **18** 1049 (1967)
17. Kondo J *Physica B (Utrecht)* **126** 377 (1984)
18. Yamada K, Sakurai A, Miyazima S, Hwang H S *Progr. Theor. Phys.* **75** 1030 (1986)
19. Leggett A J, Chakravarty S, Dorsey A T, et al. *Rev. Mod. Phys.* **59** 1 (1987)
20. Yamada K, Sakurai A, Takeshige M *Progr. Theor. Phys.* **70** 73 (1983)
21. Yamada K, Sakurai A, Miyazima S *Progr. Theor. Phys.* **73** 1342 (1985)
22. Morozov A I, Sigov A S *Izv. Akad. Nauk SSSR Ser. Fiz.* **54** 1432 (1990)
23. Morozov A I, Sigov A S *J. Phys. Cond. Matter* **3** 2867 (1991)
24. Kondo J *Physica B (Utrecht)* **84** 40 (1976)
25. Tsuzuki T *Solid State Commun.* **69** 7 (1989)
26. Tsuzuki T *Progr. Theor. Phys.* **81** 770 (1989)
27. Vladar K, Zawadowski A *Phys. Rev. B* **28** 1564, 1582, 1596 (1983)
28. Vladar K, Zawadowski A, Zimanyi G T *Phys. Rev. B* **37** 2001, 2015 (1988)
29. Alefeld G, Völkel J (Eds) *Hydrogen in Metals* 2 vols (Berlin, Springer, 1978)
30. Harrison W A *Solid State Theory* (New York: McGraw-Hill, 1970)
31. Beal–Monod M T *J. Phys. Chem. Solids* **28** 1261 (1967)
32. Zyuzin A Yu, Spivak B Z *Pis'ma Zh. Eksp. Teor. Fiz.* **43** 185 (1986) [*JETP Lett.* **43** 234 (1986)]
33. Bulaevskii L N, Panyukov S V *Pis'ma Zh. Eksp. Teor. Fiz.* **43** 190 (1986) [*JETP Lett.* **43** 240 (1986)]
34. Somenkov V A, Shil'shtein S Sh *Fazovye Prevrashcheniya Vodoroda v Metallakh* (Phase Transitions of Hydrogen in Metals) (Moscow: Institute of Atomic Energy, 1978)
35. Morozov A I, Sigov A S *Solid State Commun.* **67** 841 (1988)
36. Morozov A I, Sigov A S *Zh. Eksp. Teor. Fiz.* **95** 170 (1989) [*Sov. Phys. JETP* **68** 97 (1989)]
37. Blaschko O, Krexner G, Daou J N, Vajda P *Phys. Rev. Lett.* **55** 2876 (1985)
38. Blaschko O, Krexner G, Pleschiutschnig J, et al. *Phys. Rev. B* **39** 5605 (1989)
39. Bonnet J E, Ross D K, Faux D A, Anderson I S *J. Less-Common Met.* **129** 287 (1987)
40. McKergow M W, Ross D K, Bonnet J E, et al. *J. Phys. C* **20** 1909 (1987)
41. Blaschko O, Pleschiutschnig J, Vajda P, et al. *Phys. Rev. B* **40** 5344 (1989)
42. Daou J N, Vajda P *J. Phys. F* **12** L13 (1982)
43. Jensen C L, Zalesky M P *J. Less-Common Met.* **75** 197 (1980)
44. Bonnet J E, Juckum C, Lucasson A *J. Phys. F* **12** 699 (1982)
45. Vajda P, Daou J N, Burger K, et. al. *Phys. Rev. B* **34** 5154 (1986)
46. Sellers G J, Anderson A C, Birnbaum H K *Phys. Rev. B* **10** 2771 (1974)
47. Morkel C, Wipf H, Neumaier K *Phys. Rev. Lett.* **40** 947 (1978)
48. Wipf H, Neumaier K *Phys. Rev. Lett.* **52** 1308 (1984)
49. O'Hara S G, Sellers G J, Anderson A C *Phys. Rev. B* **10** 2777 (1974)
50. Poker D B, Setser G G, Granato A V, Birnbaum H K *Z. Phys. Chem.* (*Frankfurt am Main*) **116** 39 (1979)
51. Cannelli G, Cantelli R, Vertechi G *J. Less-Common Met.* **88** 335 (1982)
52. Cannelli G, Cantelli R, Cordero F *Phys. Rev. B* **34** 7721 (1986)
53. Bellessa G *J. Phys. Lett.* **44** L-387 (1983)
54. Poker D B, Setser G G, Granato A V, Birnbaum H K *Phys. Rev. B* **29** 622 (1984)
55. Huang K F, Granato A V, Birnbaum H K *Phys. Rev. B* **32** 2178 (1985)
56. Morr H, Muller A, Weiss G, et al. *Phys. Rev. Lett.* **63** 2084 (1989)
57. Richter D, Topler J, Springer T *J. Phys. F* **6** L-93 (1976)
58. Wipf H, Magerl A, Shapiro S M, et al. *Phys. Rev. Lett.* **46** 947 (1981)
59. Wipf H, Steinbinder D, Neumaier K, et al. *Europhys. Lett.* **4** 1379 (1987)
60. Steinbinder D, Wipf H, Magerl A, et al. *Europhys. Lett.* **6** 535 (1988)
61. Neumaier K, Steinbinder D, Wipf H, et al. *Z. Phys. B* **76** 359 (1989)

62. Wipf H *Ber. Bunsenges. Phys. Chem.* **95** 438 (1991)
63. Maschhoff K R, Granato A V *J. Phys. (Paris)* **46** *Colloq.* 10, C10–87 (1985)
64. Cannelli G, Cantelli R, Cordero F *Phys. Rev. B* **35** 7264 (1987)
65. Morozov A I, Sigov A S *Fiz. Tverd. Tela (Leningrad)* **33** 1772 (1991) [*Sov. Phys. Solid State* **33** 996 (1991)]
66. Anderson I S, Berk N F, Rush J J, et. al. *Phys. Rev. Lett.* **65** 1439 (1990)
67. Berk N F, Rush J J, Udovic T J, Anderson I S *J. Less-Common Met.* **173** 496 (1991)
68. Morozov A I, Sigov A S *Physica B* **169** 481 (1991)
69. Kondo J *Physica B+ C* **132** 303 (1985)
70. Lifshitz E M, Pitaevskii L P *Physical Kinetics* (Oxford: Pergamon Press, 1981)]
71. Morozov A I, Sigov A S *Fiz. Tverd. Tela (Leningrad)* **32** 3234 (1990) [*Sov. Phys. Solid State* **32** 1874 (1990)]
72. Pippard A B *Philos. Mag.* **46** 1104 (1955)
73. Kittel C *Quantum Theory of Solids* (New York: Wiley, 1963)
74. Abrikosov A A *Osnovy Teorii Metallov* (Fundamentals of the Theory of Metals) (Moscow: Nauka, 1987)
75. Bhatia A B, Moore R A *Phys. Rev. B* **121** 1075 (1961)
76. Morozov A I, Sigov A S *Zh. Eksp. Teor. Fiz.* **98** 1454 (1990) [*Sov. Phys. JETP* **71** 813 (1990)]
77. Morozov A I, Sigov A S *Zh. Eksp. Teor. Fiz.* **104** 2872 (1993) [*Sov. Phys. JETP* **77** 324 (1993)]